Master Thesis

Cell Coverage Extension with Orthogonal Random Precoding for Massive MIMO Systems

by

Nguyen Thanh Nhan

Department of Electrical and Information Engineering

The Graduate School

Seoul National University of Science and Technology

August 2017

Cell Coverage Extension with Orthogonal Random Precoding for Massive MIMO Systems

by

Nguyen Thanh Nhan

A Master Thesis submitted to the Department of Electrical and Information Engineering at the Graduate School Seoul National University of Science and Technology in partial fulfillment of the requirements for the degree of Master of science

July 2017

Approved by

Ji-Hoon Yun

Advisor

This certifies that the master thesis of
Nguyen Thanh Nhan is approved

Thesis Committee Chair: Prof. Taehyun Jeon

Prof. Ji-Hoon Yun (Thesis Committee Member #1)

Prof. Kyungchun Lee (Thesis Committee Member #2)

The Graduate School

Seoul National University of Science and Technology

July 2017

Contents

Abstract

Cell Coverage Extension with Orthogonal Random Precoding for Massive MIMO Systems

Nguyen Thanh Nhan

Supervisor: Ji-Hoon Yun

Dept. of Electrical and Information Engineering

Graduate School

Seoul National University of Science and Technology

This thesis investigates a coverage extension scheme based on orthogonal random precoding (ORP) for the downlink of massive multiple-input multiple-output (MIMO) systems. In this scheme, a precoding matrix consisting of orthogonal vectors is employed at the transmitter to enhance the maximum signal-to-interference-plus-noise ratio (SINR) of the user. To analyze and optimize the ORP scheme's performance, the analytical expressions of the downlink coverage probability and cell-edge sum-rate for various receiver structures are derived. It is shown that the optimal coverage performance is achieved when a small number of precoding vectors are used. The performance of the ORP scheme is further analyzed when different random precoder groups are utilized over multiple time slots to exploit precoding diversity. Numerical results show that the analytical expressions accurately capture the coverage behaviors of the systems employing the ORP scheme.

List of Figures

Chapter 1

Introduction

In mobile communication, a massive multiple-input multiple-output (MIMO) system, where the base station (BS) is equipped with a large number of antennas, has been recently considered as a potential technique for dramatically improving system performance in terms of spectral and power efficiency [1], [2]. It is also thought that a massive MIMO system is capable of extending its cell coverage by exploiting a large array gain to compensate for the significant path loss in millimeter-wave propagation channels, which provides a wider bandwidth for 5G communication systems [3]. Specifically, in the downlink, precoding techniques can be exploited to extend the cell coverage in massive MIMO systems [4].

Most studies on precoding techniques for MIMO systems have been carried out under the assumption of perfect channel state information (CSI) at the transmitter [5–7]. However, in practical systems, the CSI is imperfect [8], [9], and in frequency-division duplexing, it is typically acquired by the feedback signals from the receivers, which results in a significant overhead, especially in massive MIMO systems [10], [11]. Moreover, in contrast to unicast data channels, for multicast/broadcast channels, which must be received by a large number of mobile users in each cell, CSI-based precoding strategies can lead to the potentially excessive overhead [12], [13]. Therefore, to achieve the coverage gain in the downlink of massive MIMO systems, non- or partial-CSI based transmission techniques such as random precoding should be considered [14], [15].

1.1 Related works

There has been a line of research studying the coverage extension problem. In [16], the authors showed that the cell coverage can be extended by the dual-hop space-time relaying scheme. The results in [17] indicate that the proposed strategy called the strongest-weakest-normalized-subchannel-first scheduling can significantly expand the coverage of MIMO systems. In [18], the downlink coverage performance in MIMO heterogeneous cellular networks was investigated; furthermore, the work was extended with flexible cell selection in [19]. The same problem has also been recently considered in massive MIMO systems [20], [21]. The analytical expressions for the asymptotic coverage probability and rate for both downlink and uplink in random cellular networks with Poisson distributed BS locations are presented in [20]. The cell coverage optimization problem for the massive MIMO uplink was investigated in [21].

There has been another line of work studying random beamforming. In [12], the authors presented asymptotic throughput scaling laws for space-division multiple access with orthogonal beamforming known as per user unitary and rate control for the interference- and noise-limited regimes. The work of [13] showed that in the orthogonal random precoding (ORP) scheme, the throughput scales linearly with the number of transmit antennas N_t, provided N_t does not increase faster than $\log n$, where n is the number of users. The works of [22] and [23] investigated the achievable rates in a multi-cell setup subject to inter-cell interference and characterized the achievable degree of freedom region in the MIMO random beamforming scheme. In [24], the authors proposed the use of multiple transmit antennas with the aim of inducing channel fluctuations to exploit multiuser diversity.

1.2 Contributions

In contrast to the above mentioned approaches, this thesis focuses on an ORP scheme to enhance the cell coverage in the downlink of massive MIMO systems. As an advantage, this scheme requires only partial CSI at the transmitter. Specifically, each receiver only feeds back its maximum signal-to-interference-plus-noise ratio (SINR) and the corresponding beam index. In Chapter 3, the analytical expressions for the downlink coverage probability for two typical receiver structures: the single-antenna receiver (ORP-SA), the multiple-antenna receiver with antenna selection (ORP-AS). It is analytically and numerically shown that the optimal coverage performance is achieved when few precoding vectors are used.

Recently, the anticipated requirement of a wide spectrum for future mobile communication systems has motivated the wireless industry to consider mmWave [25]. With a small wavelength, as in mmWave, a large number of antennas can be deployed at the BS to provide beamforming gains [26]. However, in massive MIMO systems, packing a large number of antennas into limited-size mobile stations (MSs) leads to high levels of antenna correlation. Therefore, in Chapter 4 of this thesis, the investigation into the ORP scheme is also extended to mmWave massive MIMO systems under the assumption of near semi-highly correlated channels, and the minimum-mean-squared-error (MMSE) receiver are employed. We derive the approximate distribution of the maximum SINR, which allows us to derive the analytical expressions for the coverage probability and the cell-edge sum-rate. Then, we show the tradeoff between the coverage and sum-rate performance of the ORP scheme. This result reveals that a single random precoding vector is the optimal design for the ORP scheme that can provide maximum coverage. In contrast, to achieve the highest sum-rate performance, the number of precoding vectors should be as large as the number of transmit antennas.

The performance of the ORP scheme is further analyzed when different random precoder groups are utilized over multiple time slots to exploit precoding diversity. The numerical results show that the proposed ORP scheme over multiple time slots provides a substantial coverage gain over the space-time coding scheme despite its low feedback overhead. We also show that by enhancing the coverage performance while preserving a predefined sum-rate threshold, this scheme can optimize the trade-off between coverage and sum-rate performance. The contributions of this thesis are presented in more detail in [27] and [28].

Notations: Throughout this thesis, scalars, vectors, and matrices are denoted by lower-case, bold-face lower-case, and bold-face upper-case letters, respectively. The (i, j)th element of a matrix is denoted as $[\cdot]_{i,j}$, and $(\cdot)^T$ and $(\cdot)^*$ denote the transpose and conjugate transpose operators, respectively. Further, $\|\cdot\|$ denotes the norm of a vector. $\mathbf{P}\{\cdot\}$ and $\mathbf{E}\{\cdot\}$ denote probability and statistical expectation respectively. The distribution of a circularly symmetric complex Gaussian random variable with zero-mean and variance σ^2 is denoted by $\mathcal{CN}(0, \sigma^2)$, while $\chi^\eta\left(\epsilon^2\right)$ denotes the central chi-square random variable of η degrees of freedom with mean ϵ^2. Finally, $\mathbb{C}^{x\times y}$ and $\mathbb{R}_+^2$ denote the space of $x \times y$ complex matrices and the non-negative real coordinate space of two dimensions, respectively.

Chapter 2

System Model and ORP Scheme

2.1 System model

In this section, we present the system model of a downlink channel in a massive MIMO network, which is illustrated in Fig. 2.1. The BS and each mobile station (MS) have N_t

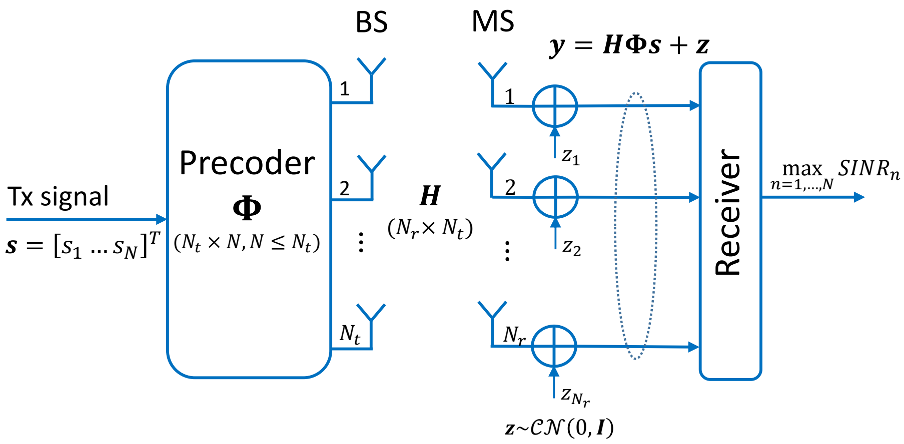

FIG. 2.1. Downlink system with orthogonal random precoding.

and N_r antennas, respectively. We assume that the channel is block-fading and is constant during a coherence interval. At time t, the received signal at the kth MS is given by

$$\boldsymbol{y}_k(t) = \boldsymbol{H}_k \boldsymbol{\Phi}(t) \boldsymbol{s}(t) + \boldsymbol{z}_k(t), \tag{2.1}$$

where $\boldsymbol{H}_k \in \mathbb{C}^{N_r \times N_t}$ is the channel coefficient matrix between the BS and the kth MS, $\boldsymbol{s}(t) \in \mathbb{C}^{N \times 1}$ is the vector of transmit symbols, $\boldsymbol{z}_k(t) \in \mathbb{C}^{N_r \times 1}$ is an additive white Gaussian noise vector in the kth MS with elements $\mathcal{CN}(0, \sigma^2)$, and $\boldsymbol{\Phi}(t) \in \mathbb{C}^{N_t \times N}$ is a random unitary matrix consisting of N orthonormal precoding vectors with the constraint $N \leq N_t$. We assume that the N elements in $\boldsymbol{s}(t)$ are the signals sent to N different MSs, indicating that N MSs are simultaneously served each time. The channel matrix is assumed to be Rayleigh fading; hence, the coefficients of $\boldsymbol{H}_k$ are independent and identically distributed (i.i.d.) Gaussian random variables, i.e., $[\boldsymbol{H}_k]_{i,j} \sim \mathcal{CN}(0, 1)$. Moreover, we assume the average total transmit power is P_T, i.e., $\mathbf{E}\left\{\boldsymbol{s}(t)^* \boldsymbol{s}(t)\right\} = P_T$, which yields that the transmit power per symbol is P_T/N, i.e., $\mathbf{E}\left\{|s_i(t)|^2\right\} = P_T/N$, where $s_i(t)$ is the ith element in $\boldsymbol{s}(t)$, $i = 1, 2, \ldots, N$. Let ρ be the average received signal-to-noise ratio (SNR); then, ρ is expressed as

$$\rho = \frac{\mathbf{E}\left\{\|\boldsymbol{\Phi}(t)\boldsymbol{s}(t)\|^2\right\}}{\sigma^2} = \frac{P_T}{\sigma^2}.$$

2.2 Orthogonal Random Precoding

In the ORP scheme for unicast data channels, the signals are precoded by N orthonormal random precoding vectors before transmission. The ORP scheme includes two phases: training and transmission, which are illustrated in Fig. 2.2.

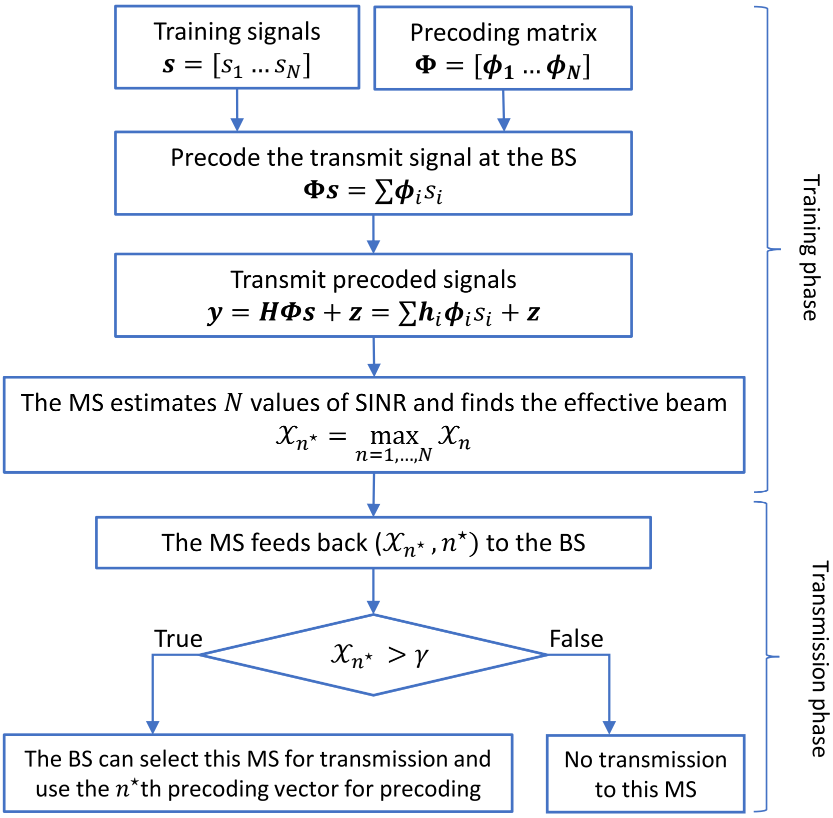

FIG. 2.2. Training and transmission phases of the ORP scheme.

2.2.1 Training phase

The BS starts the training phase by randomly generating a precoding matrix $\boldsymbol{\Phi}$ of N orthonormal precoding vectors $\boldsymbol{\phi}_1, \boldsymbol{\phi}_2, \dots, \boldsymbol{\phi}_N$. The training signals are multiplied by the precoding matrix before being sent to the MSs.

At the receiver side, each MS computes the SINR of each precoding vector and finds the maximum one. Specifically, at an MS, N SINR values $\mathcal{X}_1, \dots, \mathcal{X}_N$, which correspond to N orthogonal beams, are estimated as in the schemes of [13], [22]. If $\mathcal{X}_{n^\star}$ is determined as the maximum SINR, then the value $\mathcal{X}_{n^\star}$ as well as its index $n^\star$ are fed back to the BS. In this work, this optimally selected precoding vector is referred to as the "effective beam."

2.2.2 Transmission phase

When the training phase is finished, the BS knows the effective beam index and its SINR for each MS. Then, if the maximum SINR is higher than a predefined threshold γ, the MS is determined to be in coverage and can be selected for data transmission. In this phase, the transmit signal is precoded by the effective beam before transmission.

Similar to the unicast data channels, the ORP scheme can also be employed for multicast/broadcast channels in which it is problematic to achieve a coverage gain through multiple transmit antennas because CSI-based precoding schemes cannot be applied. As an example, in LTE/LTE-A systems, the physical broadcast channel (PBCH), which delivers the master information block to the MSs during the initial call setup procedure [29, 30], can be transmitted via random precoding vectors; however, in contrast to the unicast data channels, the training phase is not performed.

2.3 Coverage of the ORP scheme

The coverage ability of the ORP scheme is evaluated by the downlink coverage probability which can then be defined as follows:

Definition 2.1 (Downlink Coverage Probability)**.** In the downlink of a massive MIMO system using the ORP scheme, an MS is said to be in coverage if its maximum SINR is higher than a predefined threshold γ. The coverage probability is defined as

$$\mathcal{P}(\gamma, N) = \mathbf{P}\left\{\max_{n=1,\ldots,N} \mathcal{X}_n > \gamma\right\} = \mathbf{P}\left\{\mathcal{X}_{max} > \gamma\right\}. \tag{2.2}$$

Chapter 3

Cell Coverage Extension of the ORP Scheme

In this chapter, we investigate the coverage behavior of the ORP scheme in a typical massive MIMO system for two receiver structures: single antenna (SA) receivers and multiple antenna receiver with AS. The coverage ability of the ORP scheme is evaluated by the coverage probability, which is defined in Definition 2.1.

3.1 Downlink coverage probability with the ORP scheme

3.1.1 Single receive antenna system

We first consider the baseline scenario where each MS is equipped with a single receive antenna. Without loss of generality, hereafter, we drop the indexes k and t. The received signal in (2.1) becomes

$$y = \boldsymbol{h}^T \boldsymbol{\Phi} \boldsymbol{s} + z = \boldsymbol{h}^T \sum_{i=1}^{N} \boldsymbol{\phi}_i s_i + z, \tag{3.1}$$

where $\boldsymbol{h}^T \in \mathbb{C}^{1\times N_t}$ is the channel vector between the BS and single-antenna MS, and we assume that the MS estimates $\boldsymbol{h}^T\boldsymbol{\phi}_i, i = 1, \ldots, N$, by training procedures. Specifically, the SINR for $\boldsymbol{\phi}_n$ can be expressed as

$$\mathcal{X}_n = \frac{\left|\boldsymbol{h}^T\boldsymbol{\phi}_n\right|^2 \frac{P_T}{N}}{\sigma^2 + \sum_{i\neq n}^{N} \left|\boldsymbol{h}^T\boldsymbol{\phi}_i\right|^2 \frac{P_T}{N}} = \frac{\left|\boldsymbol{h}^T\boldsymbol{\phi}_n\right|^2}{\frac{N}{\rho} + \sum_{i\neq n}^{N} \left|\boldsymbol{h}^T\boldsymbol{\phi}_i\right|^2},\ n = 1, \ldots, N. \tag{3.2}$$

Theorem 3.1. *In a system employing the ORP scheme with multiple precoding vectors and a single antenna receiver (ORP-SA scheme), the downlink coverage probability is given by*

$$\mathcal{P}(\gamma, N) = \begin{cases} \frac{N}{(\gamma+1)^{N-1}} e^{-\frac{\gamma N}{\rho}}, & \gamma \geq 1 \\ \mathcal{P}(\gamma, N)_1 + \sum_{k=2}^{m-1} \mathcal{P}(\gamma, N)_k + \mathcal{P}(\gamma, N)_m, & \gamma < 1, \end{cases} \tag{3.3}$$

where $\mathcal{P}(\gamma, N)_1$, $\mathcal{P}(\gamma, N)_k$, and $\mathcal{P}(\gamma, N)_m$ are

$$\mathcal{P}(\gamma, N)_1 = \frac{N}{(N-2)!}\left(e^{-\frac{\gamma N}{\rho}} C_1 + C_2\right), \tag{3.4}$$

$$\mathcal{P}(\gamma, N)_k = \xi_k\left(e^{-\frac{\gamma N}{\rho}} \frac{\gamma^l}{l!} D_1 - \frac{1}{(k-1)^l l!} D_2\right) + \xi_k\left(\frac{1}{k^l l!} E_1 - \frac{1}{(k-1)^l l!} E_2\right), \tag{3.5}$$

$$\mathcal{P}(\gamma, N)_m = \xi_m\left(e^{-\frac{\gamma N}{\rho}} \frac{\gamma^l}{l!} F_1 - \frac{1}{(m-1)^l l!} F_2\right). \tag{3.6}$$

Here, the function $\xi_p(\cdot)$, $p = 1, \ldots, N-1$, is defined as

$$\xi_p(\cdot) = \frac{N}{(N-2)!}\sum_{t=1}^{k}\binom{N-1}{t-1}(-1)^{t+1}\sum_{i=0}^{N-2}\binom{N-2}{i}(1-t)^i i! \sum_{l=0}^{i}(\cdot), \tag{3.7}$$

and C_1, C_2, D_1, D_2, E_1, E_2, F_1, and F_2 are given as follows:

$$C_1 = \frac{(N-2)!}{(\gamma+1)^{N-1}}\left(1 - e^{-(\gamma+1)b_1}\sum_{l=0}^{N-2}\frac{(\gamma+1)^l b_1^l}{l!}\right), \tag{3.8}$$

$$C_2 = \frac{(N-2)!}{2^{N-1}} e^{-2b_1}\sum_{l=0}^{N-2}\frac{2^l b_1^l}{l!}, \tag{3.9}$$

$$\begin{aligned} D_1 = \sum_{v=0}^{l}\binom{l}{v}\left(\frac{N}{\rho}\right)^{l-v}\frac{(N-i+v-2)!}{(\gamma+1)^{N-i+v-1}} & \\ \times \sum_{u=0}^{N-i+v-2}\frac{(\gamma+1)^u}{u!}\left(e^{-(\gamma+1)b_{k-1}} b_{k-1}^u - e^{-(\gamma+1)b_k} b_k^u\right), & \end{aligned} \tag{3.10}$$

$$\begin{aligned} D_2 = \frac{(N-i+l-2)!}{\left(\frac{k}{k-1}\right)^{N-i+l-1}}\Bigg[& e^{-\frac{k}{k-1}b_{k-1}}\sum_{u=0}^{N-i+l-2}\left(\frac{k}{k-1}\right)^u \frac{b_{k-1}^u}{u!} \\ & - e^{-\frac{k}{k-1}b_k}\sum_{u=0}^{N-i+l-2}\left(\frac{k}{k-1}\right)^u \frac{b_k^u}{u!}\Bigg], \end{aligned} \tag{3.11}$$

$$E_1 = \frac{(N-i+l-2)!}{\left(\frac{k+1}{k}\right)^{N-i+l-1}} e^{-\frac{k+1}{k}b_k}\sum_{u=0}^{N-i+l-2}\left(\frac{k+1}{k}\right)^u \frac{b_k^u}{u!}, \tag{3.12}$$

$$E_2 = \frac{(N-i+l-2)!}{\left(\frac{k}{k-1}\right)^{N-i+l-1}} e^{-\frac{k}{k-1}b_k}\sum_{u=0}^{N-i+l-2}\left(\frac{k}{k-1}\right)^u \frac{b_k^u}{u!}, \tag{3.13}$$

$$F_1 = \sum_{v=0}^{l}\binom{l}{v}\left(\frac{N}{\rho}\right)^{l-v}\frac{(N-i+v-2)!}{(\gamma+1)^{N-i+v-1}} e^{-(\gamma+1)b_{m-1}}\sum_{u=0}^{N-i+v-2}(\gamma+1)^u \frac{b_{m-1}^u}{u!}, \tag{3.14}$$

$$F_2 = \frac{(N-i+l-2)!}{\left(\frac{m}{m-1}\right)^{N-i+l-1}} e^{-\frac{m}{m-1}b_{m-1}} \sum_{u=0}^{N-i+l-2} \left(\frac{m}{m-1}\right)^u \frac{b_{m-1}^u}{u!}, \tag{3.15}$$

where b_k*,* $k = 1, \ldots, N-1$*, is given as* $b_k = \frac{\gamma N}{\rho(1/k-\gamma)}$.

Proof. See Appendix A.1. □

It is observed that in the ORP scheme, $\mathcal{P}(\gamma, N)$ depends on N, the number of beams. In the ORP scheme, when the number of beams is large, the precoding diversity gain is enhanced. This increases the chances that a precoding vector out of N randomly generated orthogonal ones matches well with the channel of a user to provide high receive signal power. However, at the same time, the effective beam at an MS is affected by additional interference signals introduced by the other beams. Therefore, it is uncertain whether employing a larger number of precoding vectors leads to a better coverage performance. In Remarks 3.2–3.4, the dependencies of $\mathcal{P}(\gamma, N)$ on γ and N in the ORP scheme are stated.

Remark 3.2. For any value of γ, as N increases, the coverage probability approaches zero, i.e., $\mathcal{P}(\gamma, N) \longrightarrow 0, \text{ as } N \longrightarrow \infty, N \leq N_t, \forall \gamma$.

Proof. We observe that $\gamma\left(\frac{N}{\rho} + b\right) \longrightarrow \infty, \text{ as } N \longrightarrow \infty, \forall\gamma$. Hence, from the expression for the downlink coverage probability in (2), we have

$$\mathcal{P}(\gamma, N) = \int_0^\infty \int_{\gamma\left(\frac{N}{\rho}+b\right)}^\infty f_{A_{max},B_{min}}(a,b)\,da\,db \longrightarrow 0, \text{ as } N \longrightarrow \infty, \forall\gamma,$$

which proves Remark 3.2. □

Remark 3.3. When $\gamma \geq 1$, the downlink coverage probability is a decreasing function of N. Let $N^\star$ denote the optimal number of precoding vectors such that the ORP scheme provides the maximum coverage probability. When $\gamma \geq 1$, the maximum coverage probability becomes

$$\mathcal{P}(\gamma, N) = e^{-\frac{\gamma}{\rho}},$$

which is achieved for $N^\star = 1$[1]. Furthermore, for multiple precoders, i.e., $N \geq 2$, the higher N, the more slowly $\mathcal{P}(\gamma, N)$ decreases.

Proof. See Appendix A.2 □

Next, we consider the case of $\gamma < 1$. From (2), we see that the downlink coverage probability is determined by $f_{A_{max},B_{min}}(a, b)$ in (11) in the area

$$\mathcal{R} = \left\{ (a, b) \in \mathbb{R}_+^2 : \gamma \left(\frac{N}{\rho} + b \right) \leq a \right\}.$$

It can be seen from Fig. 3 in Appendix A.1 that when N increases, sector $\mathcal{R}$ narrows. However, $f_{A_{max},B_{min}}(a, b)$ varies depending on N. Therefore, in contrast to the case of $\gamma \geq 1$, the decreasing property is not generally secured. If $\mathcal{P}(\gamma, N)$ is not a decreasing function of N, a larger $N^\star$ can achieve the maximum $\mathcal{P}(\gamma, N)$. These properties of $\mathcal{P}(\gamma, N)$ are stated in the following remark and justified by simulation results in Section 3.2.

Remark 3.4. When $\gamma < 1$, the conclusion in Remark 3.3 on the decreasing property of the downlink coverage probability is not valid anymore; thus, the optimal value $N^\star$ can be larger than one. However, even when $\gamma < 1$, the maximum coverage is achieved for a small number of precoding vectors, i.e. $N^\star \ll N_t$.

Remarks 3.3 and 3.4 show that when a sufficiently small number of precoding vectors are employed, the coverage probability becomes higher than when N is large. Especially, when $\gamma \geq 1$, the downlink coverage probability is a decreasing function of N, which results in

[1] This does not mean that only a single user is served by the entire system. Multiple users can be simultaneously served with multiple time-frequency resources.

$N^\star = 1$. Furthermore, because the coverage probability decreases more rapidly for small N, a slight increase in N can substantially lower the coverage probability. Remarks 3.2–3.4 imply that the interference caused by the other beams affects the coverage performance more significantly than the precoding diversity gain.

Note that based on Theorem 3.1, we can readily derive the cumulative distribution function (CDF) of $\mathcal{X}_{max}$ in a baseline system where a single antenna is employed at the receiver.

Corollary 3.5. *The CDF of the random variable* $\mathcal{X}_{max} = \max\limits_{n=1,\ldots,N} \mathcal{X}_n$ *is given as*

$$F_{\mathcal{X}_{max}}(x) = \begin{cases} 1 - \frac{N}{(x+1)^{N-1}} e^{-\frac{xN}{\rho}}, & x \geq 1 \\ 1 - \left(\mathcal{P}(x,N)_1 + \sum_{k=2}^{m-1} \mathcal{P}(x,N)_k + \mathcal{P}(x,N)_m\right), & x < 1, \end{cases} \tag{3.16}$$

where $\mathcal{P}(x,N)_1$*,* $\mathcal{P}(x,N)_k$*, and* $\mathcal{P}(x,N)_m$ *are given in* (3.4)*,* (3.5)*, and* (3.6)*, respectively.*

Proof. By Definition 2.1, we have $\mathcal{P}(\gamma, N) = \mathbf{P}\left\{\mathcal{X}_{max} > \gamma\right\} = 1 - F_{\mathcal{X}_{max}}(\gamma)$, which leads to

$$F_{\mathcal{X}_{max}}(\gamma) = 1 - \mathcal{P}(\gamma, N). \tag{3.17}$$

From (3.3) and (3.17), we obtain the CDF of $\mathcal{X}_{max}$ in (3.16). □

3.1.2 Receivers with AS

In an AS receiver, multiple receive antennas are utilized to achieve receive spatial diversity gains. The downlink coverage probability of an AS receiver in a system employing the ORP scheme is given in the following theorem.

Theorem 3.6. *The downlink coverage probability of the ORP scheme with an AS receiver (ORP-AS) is*

$$\mathcal{P}(\gamma,N)_{AS}=\begin{cases}1-\left(1-\frac{N}{(\gamma+1)^{N-1}}e^{-\frac{\gamma N}{\rho}}\right)^{N_r}, & \gamma\geq 1\\ 1-\left[1-\left(\mathcal{P}(\gamma,N)_1+\sum_{k=2}^{m-1}\mathcal{P}(\gamma,N)_k+\mathcal{P}(\gamma,N)_m\right)\right]^{N_r}, & \gamma<1,\end{cases}\tag{3.18}$$

where $\mathcal{P}(\gamma,N)_1$, $\mathcal{P}(\gamma,N)_k$, *and* $\mathcal{P}(\gamma,N)_m$ *are given in* (3.4), (3.5), *and* (3.6), *respectively.*

Proof. Let $\mathcal{X}_{max}^{AS}$ denote the maximum SINR in the ORP-AS scheme, i.e.,

$$\mathcal{X}_{max}^{AS}=\max_{\substack{n=1,\dots,N\\ r=1,\dots,N_r}}\mathcal{X}_{n,r},$$

where $\mathcal{X}_{n,r}$ is the SINR for the nth beam at the rth antenna of the AS receiver. Because the channel between each pair of transmit and receive antennas are statistically independent, the SINRs at different receive antennas are i.i.d. random variables. Therefore, the CDF of $\mathcal{X}_{max}^{AS}$ is given as

$$F_{\mathcal{X}_{max}^{AS}}(\gamma)=\left[F_{\mathcal{X}_{max}}(\gamma)\right]^{N_r}.\tag{3.19}$$

Hence, we obtain

$$\mathcal{P}(\gamma,N)_{AS}=1-\mathbf{P}\left\{\mathcal{X}_{max}^{AS}>\gamma\right\}=1-F_{\mathcal{X}_{max}^{AS}}(\gamma)=1-\left[F_{\mathcal{X}_{max}}(\gamma)\right]^{N_r}.\tag{3.20}$$

From (3.16) and (3.20), the theorem is proved. □

From Theorem 3.6, it is clear that for a fixed γ and ρ, $\mathcal{P}(\gamma,N)$ depends on not only on N but also on N_r. Larger number of receive antennas mean that more spatial diversity gains can be exploited, which can increase the maximum SINR; hence, higher $\mathcal{P}(\gamma,N)$ is expected. In the following remark, the coverage performance improvement of the ORP-AS scheme and its dependence on N and N_r are presented.

Remark 3.7. In the ORP-AS scheme, the downlink coverage probability is an increasing function of N_r. In particular, in massive MIMO systems with the ORP-AS scheme that employ a fixed number of precoding vectors, the user is in coverage with a high probability provided that the system is equipped with a sufficiently large number of antennas, i.e.,

$$\mathcal{P}(\gamma, N)_{AS} \longrightarrow 1 \text{ as } N_r \longrightarrow \infty, N = c.$$

where c represents a constant.

Proof. With a fixed value of N, we observe that $0 < F_{\mathcal{X}_{max}}(\gamma) < 1$, which leads to $[F_{\mathcal{X}_{max}}(\gamma)]^{N_r} < F_{\mathcal{X}_{max}}(\gamma)$, and $[F_{\mathcal{X}_{max}}(\gamma)]^{N_r}$ is a decreasing function of N_r. Therefore, $\mathcal{P}(\gamma, N)_{AS}$ in (3.20) becomes an increasing function of N_r, and $\mathcal{P}(\gamma, N)_{AS} \longrightarrow 1,$ as $N_r \longrightarrow \infty$. Remark 3.7 is hence proved. □

3.2 Numerical results

Computer simulations were performed to evaluate the performance of the proposed ORP scheme. An orthonormal precoding matrix is created by computing an orthonormal basis for the column space of a randomly generated matrix. Furthermore, the coefficients of the channel matrix are randomly generated as $\mathcal{CN}(0, 1)$ random variables but fixed over D time slots. The values of N_t, N_r, N, D, ρ, and γ are differently assumed in each simulation.

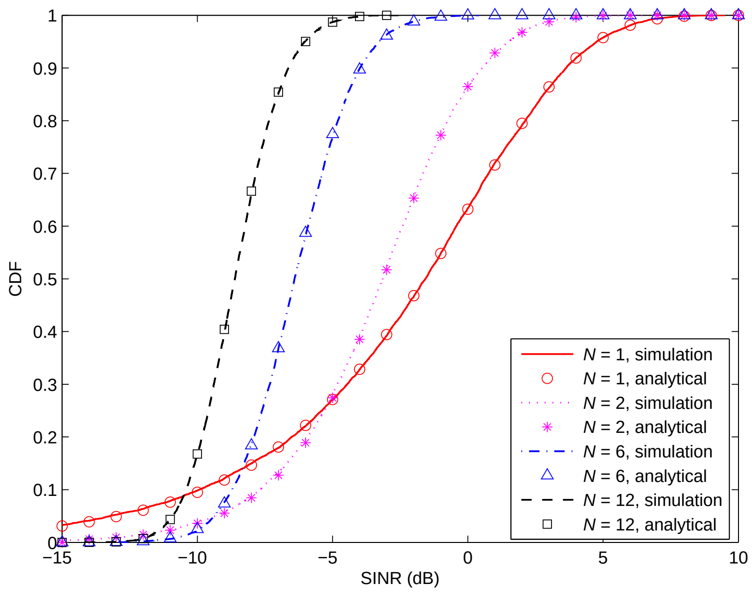

FIG. 3.1. Comparison between analytical and simulation CDFs of the maximum SINR for $\rho = 0$ dB, $N_t = 32$, $N_r = 1$, and $N \in \{1, 2, 6, 12\}$.

First, in Fig. 3.1 we validate the accuracy of the analytical CDF of the maximum SINR in the ORP scheme, which is given in Corollary 3.5, by comparing it to the simulation results. It is clear that the analytical results in (3.16) match well with the simulation results.

Figs. 3.2 and 3.3 present the results of the downlink coverage probability of the ORP-SA scheme ($N_r = 1$) to validate the accuracy of the analytical expression of $\mathcal{P}(\gamma, N)$ in Theorem 3.1. In Fig. 3.2, the case $\gamma \geq 1$ is considered, while Fig. 3.3 depicts $\mathcal{P}(\gamma, N)$ for $\gamma < 1$. In each figure, ρ is fixed, while various values of γ are assumed. In Figs. 3.2 and 3.3, it is clear that the results from the formula in Theorem 3.1 agree with those from the simulations. It can also be observed that as γ decreases, the coverage performance is significantly improved. Furthermore, as N increases, as stated in Remark 3.2, $\mathcal{P}(\gamma, N)$ approaches zero and becomes substantially smaller than it is for small N. It is clear that the optimal number of precoding vectors $N^{\star}$ depends on γ and ρ.

Specifically, in Fig. 3.2, where the higher-than-one SINR threshold, $\gamma \in \{0, 2, 4, 8\}$ dB are

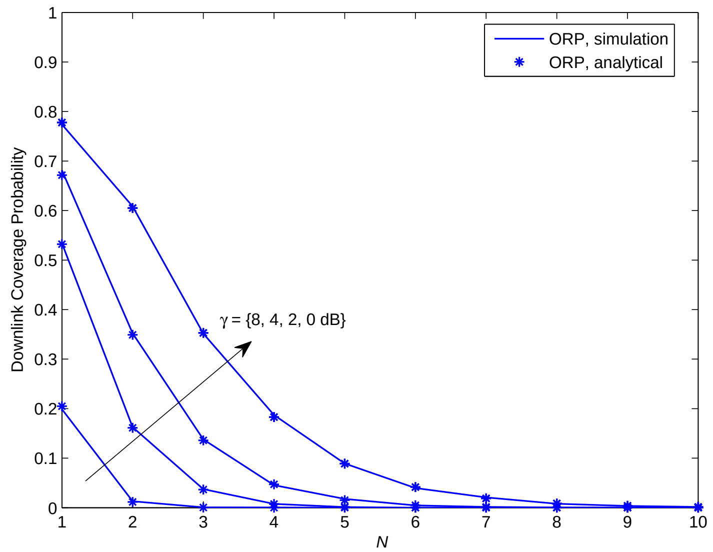

Fig. 3.2. Downlink coverage probability versus N when $\gamma \geq 1$ for $N_t = 32$, $N_r = 1$, $\rho = 6$ dB, and $\gamma \in \{0, 2, 4, 8\}$ dB.

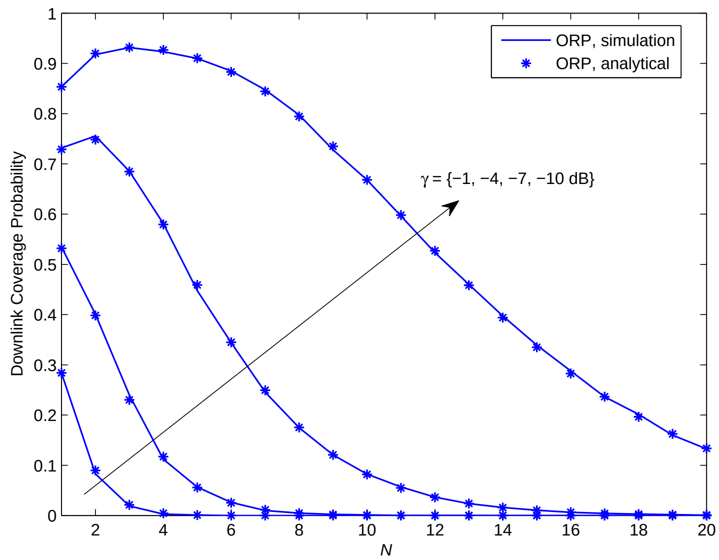

Fig. 3.3. Downlink coverage probability versus N when $\gamma < 1$ for $N_t = 32$, $N_r = 1$, $\rho = -2$ dB, and $\gamma \in \{-1, -4, -7, -10\}$ dB.

considered, it can be observed that the downlink coverage probability is a strictly decreasing function of N; thus, $\mathcal{P}(\gamma, N)$ is always maximum at $N^\star = 1$, and rapidly decreases to zero as N grows. This result implies that when $\gamma \geq 1$, the coverage performance is seriously affected by the interference from ineffective beams rather than benefiting from

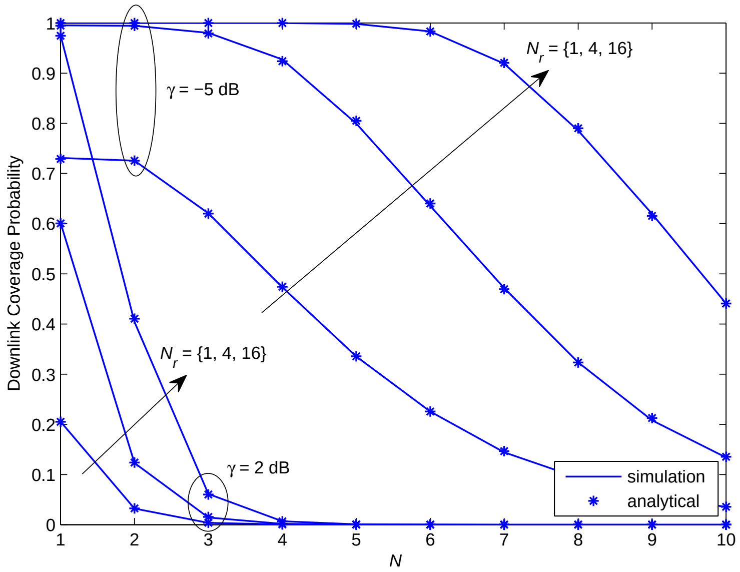

FIG. 3.4. Comparison between ORP-SA and ORP-AS for $N_t = 32$, $N_r \in \{1, 4, 16\}$, $\rho = 0$ dB, and $\gamma \in \{-5, 2\}$ dB.

the diversity gains. Another observation from Fig. 3.2 is that for $N \geq 2$, the higher N is, the more slowly $\mathcal{P}(\gamma, N)$ decreases, as discussed in Remark 3.3.

Fig. 3.3 shows the downlink coverage probability for $\gamma < 1$. Compared to the results in Fig. 3.2, it can be observed that for $\gamma < 1$, $\mathcal{P}(\gamma, N)$ is not generally a decreasing function of N. It is interesting to note that when γ becomes substantially smaller, the optimal point $N^\star$ tends to be a larger value. Therefore, the coverage performance in the massive MIMO downlink with substantially small γ can be improved by using multiple precoding vectors. However, in the assumed environments, $N^\star$ is not larger than three. Furthermore, after achieving its peak at a relatively small N, $\mathcal{P}(\gamma, N)$ approaches zero, which further proves that the use of a large number of beams is not desirable for optimizing cell coverage.

Fig. 3.4 presents the coverage performance of the ORP-AS scheme to numerically verify Theorem 3.6. In this figure, the simulation and analytical results of the downlink coverage probability match well for all cases of γ, N, and N_r. We compare $\mathcal{P}(\gamma, N)$ of the ORP-SA and ORP-AS schemes. It is clear that the ORP-AS scheme provides a significantly better coverage performance than the ORP-SA scheme. For example, for $\gamma = -5$ dB, in the ORP-AS scheme with $N_r = 16$ and $N \in [1; 6]$, $\mathcal{P}(\gamma, N) \approx 1$ is achieved; however, for the ORP-SA scheme, the maximum coverage probability is only 0.73 at $N = 1$.

Chapter 4

Coverage and Sum-rate of mmWave Massive MIMO Systems with ORP Schemes and MMSE Receivers

In this chapter, the investigation into the ORP scheme is extended to mmWave massive MIMO systems under the assumption of near semi-highly correlated channels, and MMSE receiver is employed. The expressions for coverage probability and the cell-edge sum-rate of mmWave massive MIMO systems employing the ORP scheme are derived. Based on that, we show the tradeoff between the coverage and sum-rate performance of the ORP scheme.

4.1 Distribution of the maximum SINR in mmWave massive MIMO

In this section, we derive the asymptotic cumulative density function (CDF) and probability density function (PDF) of the maximum SINR.

4.1.1 Spatially correlated channel in mmWave massive MIMO

We employ the Kronecker model to express the spatially correlated MIMO channel matrix between the BS and an MS in a massive MIMO system as follows:

$$\boldsymbol{H} = [\boldsymbol{R}_r(\varepsilon_r)]^{\frac{1}{2}} \boldsymbol{H}_w [\boldsymbol{R}_t(\varepsilon_t)]^{\frac{1}{2}},$$

where $\boldsymbol{H}_w \sim \mathcal{CN}(0, \boldsymbol{I})$, and $\boldsymbol{R}_r(\varepsilon_r)$ and $\boldsymbol{R}_t(\varepsilon_t)$ are the spatial correlation matrices at the MS and BS with correlation coefficients ε_r and ε_t ($0 \leq \varepsilon_r, \varepsilon_t \leq 1$), respectively. In mmWave communications, a large number of antennas can easily be employed because of the small wavelengths of millimeter waves [31]. At the BS, the distances between adjacent antennas can be assumed to be significantly larger than these wavelengths owing to their allowable sizes. However, large, tightly packed antenna arrays result in high levels of antenna correlation at the MS owing to its limited size [26],[32]. Therefore, in this work, we consider a near semi-highly correlated channel, where the channel correlation is assumed to be low at the transmitter and high at the receiver i.e., $\varepsilon_t \ll \varepsilon_r$. Consequently, $\boldsymbol{R}_t(\varepsilon_t) \approx \boldsymbol{I}$, and the channel matrix can be expressed as

$$\boldsymbol{H} \approx [\boldsymbol{R}_r(\varepsilon_r)]^{\frac{1}{2}} \boldsymbol{H}_w. \tag{4.1}$$

4.1.2 Approximate distribution of the maximum SINR

Without loss of generality, hereafter, we drop the time index t and denote $\tilde{\boldsymbol{H}} = \boldsymbol{H}\boldsymbol{\Phi}, \tilde{\boldsymbol{H}} \in \mathbb{C}^{N_t \times N}$. The received signal in (2.1) becomes

$$\boldsymbol{y} = \tilde{\boldsymbol{H}}\boldsymbol{s} + \boldsymbol{z}. \tag{4.2}$$

Let $\tilde{\boldsymbol{h}}_n \in \mathbb{C}^{N_t \times 1}, n = 1, \ldots, N$, be the effective channel for s_n, which can be written as $\tilde{\boldsymbol{h}}_n = \boldsymbol{H}\boldsymbol{\phi}_n$, where $\boldsymbol{\phi}_n$ represents the nth column of $\boldsymbol{\Phi}$. By denoting $\boldsymbol{W} = \tilde{\boldsymbol{H}}_{-n}\tilde{\boldsymbol{H}}_{-n}^H$, the SINR for $\boldsymbol{\phi}_n$ at the output of the MMSE receiver can be expressed as

$$\mathcal{X}_{n,\text{MMSE}} = \frac{\rho}{N}\tilde{\boldsymbol{h}}_n^H \left(\frac{\rho}{N}\boldsymbol{W} + \boldsymbol{I}\right)^{-1} \tilde{\boldsymbol{h}}_n \ , \tag{4.3}$$

where ρ is the average SNR. Owing to the large propagation loss of mmWave communications, we assume that ρ is extremely low for the cell-edge MSs. The eigenvalue decomposition of $\boldsymbol{W}$ in (4.3) can be expressed as

$$\boldsymbol{W} = \boldsymbol{Q}^H \boldsymbol{\Lambda} \boldsymbol{Q},$$

where $\boldsymbol{Q}$ is a unitary matrix and $\boldsymbol{\Lambda}$ is the diagonal matrix such that

$$\boldsymbol{\Lambda} = \begin{cases} \text{diag}\{\lambda_1, \lambda_2, \ldots, \lambda_{N-1}, \underbrace{0, \ldots, 0}_{N_r - N + 1 \text{ zeros}}\}, & N \leq N_r \\ \\ \text{diag}\{\lambda_1, \lambda_2, \ldots, \lambda_{N_r}\}, & N > N_r, \end{cases} \tag{4.4}$$

where λ_i is the ith positive eigenvalue of $\boldsymbol{W}$. From (4.3) and (4.4), $\mathcal{X}_{n,\mathrm{MMSE}}$ can be expressed as [33]

$$
\begin{aligned}
\mathcal{X}_{n,\mathrm{MMSE}} &= \tilde{\boldsymbol{h}}_n^H \left(\boldsymbol{Q}^H \boldsymbol{\Lambda} \boldsymbol{Q} + \frac{N}{\rho} \boldsymbol{I} \right)^{-1} \tilde{\boldsymbol{h}}_n \\
&= \begin{cases} \left[\bar{h}_{1,n}^*, \ldots, \bar{h}_{N_r,n}^*\right] \times \left[\frac{\bar{h}_{1,n}}{\lambda_1 + \frac{N}{\rho}}, \ldots, \frac{\bar{h}_{N-1,n}}{\lambda_{N-1} + \frac{N}{\rho}}, \frac{\bar{h}_{N,n}}{\frac{N}{\rho}}, \ldots, \frac{\bar{h}_{N_r,n}}{\frac{N}{\rho}} \right]^T, & N \leq N_r \\ \left[\bar{h}_{1,n}^*, \ldots, \bar{h}_{N_r,n}^*\right] \times \left[\frac{\bar{h}_{1,n}}{\lambda_1 + \frac{N}{\rho}}, \ldots, \frac{\bar{h}_{N_r,n}}{\lambda_{N_r} + \frac{N}{\rho}} \right]^T, & N > N_r \end{cases} \\
&= \begin{cases} \sum_{i=1}^{N-1} \frac{\left|\bar{h}_{i,n}\right|^2}{\lambda_i + \frac{N}{\rho}} + \frac{\rho}{N} \sum_{i=N}^{Nr} \left|\bar{h}_{i,n}\right|^2, & N \leq N_r \\ \sum_{i=1}^{N_r} \frac{\left|\bar{h}_{i,n}\right|^2}{\lambda_i + \frac{N}{\rho}}, & N > N_r, \end{cases}
\end{aligned} \tag{4.5}
$$

where $\bar{h}_{i,n}, i = 1, \ldots, N_r$, is the ith element of the vector $\bar{\boldsymbol{h}}_n = \boldsymbol{Q}\tilde{\boldsymbol{h}}_n$. Intuitively, in the highly correlated channel, the Wishart matrix $\boldsymbol{W}$ has a small number of *dominant* (non-negligible) eigenvalues, while the others are much smaller than them. We denote the number of dominant eigenvalues among the eigenvalues of $\boldsymbol{W}$ as η. In order to derive the distribution of the maximum SINR in the ORP scheme, we consider two cases as follows:

- **Case 1:** $N \leq N_r$

There are $N-1$ positive eigenvalues of $\boldsymbol{W}$. If these eigenvalues are arranged in the increasing order, i.e., $\lambda_{[1]} < \lambda_{[2]} < \ldots < \lambda_{[N-1]}$, we can write

$$\lambda_{[1]} < \ldots < \lambda_{[N-1-\eta]} \ll \lambda_{[N-\eta]} < \ldots < \lambda_{[N-1]}. \tag{4.6}$$

Furthermore, with the assumption of an extremely low average SNR for the cell-edge users, i.e., $\rho \to 0$, we have $\frac{N}{\rho} \gg 1$. Hence, there will be $N-1-\eta$ eigenvalues which are sufficiently lower than $\frac{N}{\rho}$, i.e.,

$$\lambda_{[1]} < \ldots < \lambda_{[N-1-\eta]} \ll \frac{N}{\rho}. \tag{4.7}$$

From (4.5)–(4.7), as $\frac{N}{\rho} \longrightarrow \infty$, we have

$$\sum_{i=1}^{N-1-\eta} \frac{\left|\bar{h}_{[i],n}\right|^2}{\lambda_{[i]} + \frac{N}{\rho}} \approx \frac{\rho}{N} \sum_{i=1}^{N-1-\eta} \left|\bar{h}_{[i],n}\right|^2, \tag{4.8}$$

and

$$\sum_{i=N-\eta}^{N-1} \frac{\left|\bar{h}_{[i],n}\right|^2}{\lambda_{[i]} + \frac{N}{\rho}} \approx 0. \tag{4.9}$$

From (4.5), (4.8), and (4.9), the SINR at the output of the MMSE receiver can be approximated as

$$\mathcal{X}_{n,\mathrm{MMSE}} \approx \frac{\rho}{N} \left(\sum_{i=1}^{N-1-\eta} \left|\bar{h}_{[i],n}\right|^2 + \sum_{i=N}^{Nr} \left|\bar{h}_{[i],n}\right|^2 \right). \tag{4.10}$$

- **Case 2:** $N > N_r$

In this case, the matrix $\boldsymbol{W}$ has a total of N_r positive eigenvalues. By arranging these eigenvalues in the increasing order and by the same manner as in (4.6) and (4.7), we get

$$\sum_{i=1}^{N_r-\eta} \frac{\left|\bar{h}_{[i],n}\right|^2}{\lambda_{[i]} + \frac{N}{\rho}} \approx \frac{\rho}{N} \sum_{i=1}^{N_r-\eta} \left|\bar{h}_{[i],n}\right|^2, \tag{4.11}$$

and

$$\sum_{i=N_r-\eta+1}^{N_r} \frac{\left|\bar{h}_{[i],n}\right|^2}{\lambda_{[i]} + \frac{N}{\rho}} \approx 0. \tag{4.12}$$

Similar to the case of $N \leq N_r$, from (4.5), (4.11), and (4.12), we have

$$\mathcal{X}_{n,\mathrm{MMSE}} \approx \frac{\rho}{N} \sum_{i=1}^{N_r-\eta} \left|\bar{h}_{[i],n}\right|^2. \tag{4.13}$$

For the general case that $N \leq N_t$ and the eigenvalues are ordered arbitrarily, we can write

$$\mathcal{X}_{n,\mathrm{MMSE}} \approx \frac{\rho}{N}\left(\sum_{i=1, i\notin \boldsymbol{\Omega}}^{Nr} \left|\bar{h}_{i,n}\right|^2\right),$$

where $\boldsymbol{\Omega}$ is the set of indices of η dominant eigenvalues. It is worth noting that because λ_i is the eigenvalue of $\boldsymbol{W} = \tilde{\boldsymbol{H}}_{-n}^H \tilde{\boldsymbol{H}}_{-n}$ while $\tilde{\boldsymbol{H}}_{-n}$ does not contain $\tilde{\boldsymbol{h}}_n$, $\left|\bar{h}_{i,n}\right|^2$ and λ_i are independent. In other words, the condition $i \notin \boldsymbol{\Omega}$ does not affect the distribution of $\left|\bar{h}_{i,n}\right|^2$. Furthermore, $\sum_{i=1,i\notin\boldsymbol{\Omega}}^{Nr} \left|\bar{h}_{i,n}\right|^2$ and $\sum_{i=1}^{Nr-\eta} \left|\bar{h}_{i,n}\right|^2$ are random variables with the same distribution. Therefore, we can write

$$\mathcal{X}_{n,\mathrm{MMSE}} \overset{d}{\approx} \frac{\rho}{N}\left(\sum_{i=1}^{Nr-\eta} \left|\bar{h}_{i,n}\right|^2\right), \tag{4.14}$$

where the symbol "$\overset{d}{\approx}$" means that the random variables on the left- and right-hand sides of the equation have approximately the same distribution. We denote the random variable $\mathcal{X}_{max,\mathrm{MMSE}}$ as the maximum SINR among N values i.e., $\mathcal{X}_{max,\mathrm{MMSE}} = \max_{n=1,\ldots,N}\left\{\mathcal{X}_{n,\mathrm{MMSE}}\right\}$. From (4.14), we have

$$\mathcal{X}_{max,\mathrm{MMSE}} \approx \frac{\rho}{N} \max_{n=1,\ldots,N}\left\{\sum_{i=1}^{Nr-\eta} \left|\bar{h}_{i,n}\right|^2\right\}. \tag{4.15}$$

Theorem 4.1. *The approximate CDF and PDF of the random variable $\mathcal{X}_{max,MMSE}$ are given as*

$$F_{\mathcal{X}_{max,MMSE}}(x) \approx \left(\sum_{k=1}^{N_r-\eta} \frac{1-e^{-\frac{N}{\rho\xi_k}x}}{\prod_{i=1,i\neq k}^{N_r-\eta}\left(1-\frac{\xi_i}{\xi_k}\right)}\right)^N \tag{4.16}$$

$$f_{\mathcal{X}_{max,MMSE}}(x) \approx \left(\sum_{k=1}^{N_r-\eta} \frac{1-e^{-\frac{N}{\rho\xi_k}x}}{\prod_{i=1,i\neq k}^{N_r-\eta}\left(1-\frac{\xi_i}{\xi_k}\right)}\right)^{N-1} \sum_{j=1}^{N_r-\eta} \frac{N^2 e^{-\frac{N}{\rho\xi_j}x}}{\prod_{i=1,i\neq j}^{N_r-\eta}\left(1-\frac{\xi_i}{\xi_j}\right)}, \tag{4.17}$$

where $\xi_j, j = 1,2,\ldots,N_r-\eta$, is the jth diagonal element of $\boldsymbol{\Psi}$ that satisfies $\bar{\boldsymbol{R}}_r(\varepsilon_r) =$

$\boldsymbol{U}\boldsymbol{\Psi}\boldsymbol{U}^H$ *with* $\bar{\boldsymbol{R}}_r(\varepsilon_r)$ *being the covariance matrix corresponding to the channel coefficients in* (4.15).

Proof. See Appendix B.3. □

It is worth noting that the value η depends on the channel correlation, number of receive antennas N_r, and number of precoding vectors N. As the correlation at the receivers increases, the number of dominant eigenvalues of $\boldsymbol{W}$ decreases significantly, i.e., $\eta \longrightarrow 1$ as $\varepsilon_r \longrightarrow 1$. In contrast, a larger η is required if N_r increases significantly, because a large increase enhances the number of dominant eigenvalues of $\boldsymbol{W}$. Furthermore, as the matrix $\boldsymbol{W}$ has at least $N-1$ positive eigenvalues in total, and η values among them are dominant, a larger N can lead to a larger η. However, since the number of dominant eigenvalues is extremely small in highly correlated channels, we can assume $\eta \ll N-1$.

4.2 Coverage probability and sum-rate analysis

4.2.1 Coverage probability

Remark 4.2. In mmWave massive MIMO systems employing the ORP scheme with MMSE receivers, the downlink coverage probability is approximated by

$$\mathcal{P}(\gamma, N) \approx 1 - \left(\sum_{k=1}^{N_r-\eta} \frac{1 - e^{-\frac{N}{\rho \xi_k}\gamma}}{\prod_{i=1, i\neq k}^{N_r-\eta} \left(1 - \frac{\xi_i}{\xi_k}\right)} \right)^N . \tag{4.18}$$

Proof. From the definition of the downlink coverage probability, we have

$$\mathcal{P}(\gamma, N) = 1 - \mathbf{P}\left\{\mathcal{X}_{max,\mathrm{MMSE}} \leq \gamma\right\} = 1 - F_{\mathcal{X}_{max,\mathrm{MMSE}}}(\gamma) \tag{4.19}$$

We insert (4.16) into (4.19), and the proof is complete. □

Theorem 4.3. *The optimal design of the ORP scheme in terms of coverage employs a single precoding vector. In other words, the optimal number of precoding vectors $N^\star$ that maximizes the downlink coverage probability is 1.*

$$N^\star = \underset{N}{\mathrm{argmax}}\left\{\mathcal{P}(\gamma, N)\right\} = 1.$$

Proof. From (43) and (4.19), we have

$$\mathcal{P}(\gamma, N) = 1 - F_{\mathcal{Y}_{max}}\left(\frac{N}{\rho}\gamma\right) = 1 - \left[F_{\mathcal{Y}}\left(\frac{N}{\rho}\gamma\right)\right]^N. \tag{4.20}$$

Hence,

$$\frac{\partial}{\partial N}\mathcal{P}(\gamma, N) = -N\left[F_{\mathcal{Y}}\left(\frac{N}{\rho}\gamma\right)\right]^{N-1}\frac{\partial}{\partial N}F_{\mathcal{Y}}\left(\frac{N}{\rho}\gamma\right). \tag{4.21}$$

As N and $F_{\mathcal{Y}}\left(\frac{N}{\rho}\gamma\right)$ are nonnegative, $\frac{\partial}{\partial N}\mathcal{P}(\gamma, N)$ has the same sign as $\frac{\partial}{\partial N}F_{\mathcal{Y}}\left(\frac{N}{\rho}\gamma\right)$. From (39), we have

$$F_{\mathcal{Y}}\left(\frac{N}{\rho}\gamma\right) = \sum_{k=1}^{N_r-\eta}\frac{1 - e^{-\frac{N\gamma}{\rho\xi_k}}}{\prod_{i=1,i\neq k}^{N_r-\eta}\left(1 - \frac{\xi_i}{\xi_k}\right)}. \tag{4.22}$$

Note that here η depends on N. Hence, $N_r - \eta$ in (4.22) is a function of N. Applying the Leibniz integral rule, we have

$$\begin{aligned}\frac{\partial}{\partial N} F_{\mathcal{Y}}\left(\frac{N}{\rho}\gamma\right) &= \frac{\partial}{\partial N}\left(\sum_{k=1}^{N_r-\eta} \frac{1-e^{-\frac{N\gamma}{\rho\xi_k}}}{\prod_{i=1,i\neq k}^{N_r-\eta}\left(1-\frac{\xi_i}{\xi_k}\right)}\right) \\ &= \left(\sum_{k=1}^{N_r-\eta} \frac{e^{-\frac{\gamma}{\xi_k}\frac{N}{\rho}}}{\xi_k \prod_{i=1,i\neq k}^{N_r-\eta}\left(1-\frac{\xi_i}{\xi_k}\right)} \frac{\gamma}{\rho}\right) - \frac{1-e^{-\frac{\eta\gamma}{\rho\xi_k}}}{\prod_{i=1,i\neq k}^{N_r-\eta}\left(1-\frac{\xi_i}{\xi_k}\right)} \frac{\partial \eta}{\partial N}. \end{aligned} \tag{4.23}$$

In Section 4.1.2, we showed that $\eta \ll N-1$. Furthermore, η grows slowly as N increases, and an increase in N does not always lead to an increase in η, which is illustrated numerically in Fig. 4.1. Therefore, we have an approximation of $\frac{\partial \eta}{\partial N} \approx 0$, which implies that the second term in (4.23) can be ignored. Finally, we can obtain

$$\frac{\partial}{\partial N} F_{\mathcal{Y}}\left(\frac{N}{\rho}\gamma\right) \approx \sum_{k=1}^{N_r-\eta} \frac{e^{-\frac{\gamma}{\xi_k}\frac{N}{\rho}}}{\xi_k \prod_{i=1,i\neq k}^{N_r-\eta}\left(1-\frac{\xi_i}{\xi_k}\right)} \frac{\gamma}{\rho}. \tag{4.24}$$

Obviously, $\frac{N}{\rho}$ and $\frac{\gamma}{\rho}$ in (4.24) are both positive. By comparing (4.24) to the PDF of $\mathcal{Y}$ in (38), we can conclude that $\frac{\partial}{\partial N} F_{\mathcal{Y}}\left(\frac{N}{\rho}x\right)$ is nonnegative. From (4.21), we have $\frac{\partial}{\partial N}\mathcal{P}(\gamma, N) \geq 0$, which means that $\mathcal{P}(\gamma, N)$ is maximized at $N^\star = 1$. □

Theorem 4.3 shows that the downlink coverage probability is a decreasing function of N, and the optimal coverage is obtained when the transmit signal is precoded by only one precoding vector, i.e., $N^\star = 1$. This implies that the interference caused by other beams affects the coverage performance more than the precoding diversity gain does. In the next subsection, we investigate the performance of the ORP scheme in terms of the sum-rate of cell-edge users.

4.2.2 Sum-rate of cell-edge users

In the following analysis, we derive the analytical expression for the sum-rate of N cell-edge MSs and examine how the sum-rate is affected by the ORP scheme.

Remark 4.4. In the transmission phase of the ORP scheme, the sum-rate of N MSs in the cell edge is approximated by

$$\mathcal{R}(N) \approx \sum_{j=1}^{N_r-\eta} \frac{N^3}{\prod_{i=1,i\neq j}^{N_r-\eta}\left(1-\frac{\xi_i}{\xi_j}\right)} \int_0^\infty \log(1+x)\, e^{-\frac{N}{\rho\xi_j}x} \left(\sum_{k=1}^{N_r-\eta} \frac{1-e^{-\frac{N}{\rho\xi_k}x}}{\prod_{i=1,i\neq k}^{N_r-\eta}\left(1-\frac{\xi_i}{\xi_k}\right)}\right)^{N-1} dx. \tag{4.25}$$

Proof. In the transmission phase, the MSs receive signals that are precoded by their effective beams. Therefore, the SINR at the output of the MMSE receivers is maximized. Hence, the sum-rate of N cell-edge MSs is given by

$$\mathcal{R}(N) \approx \mathbf{E}\left\{\sum_{j=1}^{N} \log\left(1+\mathcal{X}_{max,\mathrm{MMSE}}^{(j)}\right)\right\} = N\mathbf{E}\left\{\log\left(1+\mathcal{X}_{max,\mathrm{MMSE}}\right)\right\}, \tag{4.26}$$

where $\mathcal{X}_{max,\mathrm{MMSE}}^{(j)}$ is the maximum SINR at the jth MS. Note that "≈" is used in (4.26) instead of "=" since there is a possibility that the jth precoding vector may be the effective beam for more than one MS. However, this probability can be ignored when there are a sufficiently large number of MSs so that the MSs with the same effective beam do not need to be scheduled simultaneously. By using the PDF of $\mathcal{X}_{max,\mathrm{MMSE}}$ in Theorem 4.1, we obtain

$$\begin{aligned}\mathcal{R}(N) &\approx N\int_0^\infty \log(1+x)\, f_{\mathcal{X}_{max,\mathrm{MMSE}}}(x)dx \\ &= N\int_0^\infty \log(1+x)\left(\sum_{j=1}^{N_r-\eta} \frac{N^2 e^{-\frac{N}{\rho\xi_j}x}}{\prod_{i=1,i\neq j}^{N_r-\eta}\left(1-\frac{\xi_i}{\xi_j}\right)}\right)\left(\sum_{k=1}^{N_r-\eta} \frac{1-e^{-\frac{N}{\rho\xi_k}x}}{\prod_{i=1,i\neq k}^{N_r-\eta}\left(1-\frac{\xi_i}{\xi_k}\right)}\right)^{N-1} dx\end{aligned}$$

$$= \sum_{j=1}^{N_r-\eta} \frac{N^3}{\prod_{i=1,i\neq j}^{N_r-\eta}\left(1-\frac{\xi_i}{\xi_j}\right)} \int_0^{\infty} \log\left(1+x\right) e^{-\frac{N}{\rho\xi_j}x} \left(\sum_{k=1}^{N_r-\eta} \frac{1-e^{-\frac{N}{\rho\xi_k}x}}{\prod_{i=1,i\neq k}^{N_r-\eta}\left(1-\frac{\xi_i}{\xi_k}\right)}\right)^{N-1} dx,$$

which is the sum-rate expression given in (4.25), and the proof is complete. □

Theorem 4.5. *With the constraint $N \leq N_t$, the optimal design of the ORP scheme in terms of cell-edge sum-rate performance is an $N_t \times N_t$ random precoding matrix, i.e.,*

$$N^{\star} = \underset{N}{\operatorname{argmax}} \left\{\mathcal{R}(N)\right\} = N_t.$$

Proof. See Appendix B.4. □

Theorem 4.3 and Theorem 4.5 demonstrate the contradiction of optimizing both the coverage and sum-rate performance in the design of ORP schemes. This tradeoff will be further discussed in the next section.

4.2.3 Coverage versus cell-edge sum-rate

Remark 4.6. There is a tradeoff between the coverage performance and the cell-edge sum-rate of the ORP scheme. More specifically, an ORP scheme with a smaller number of precoding vectors extends the coverage area of the BS but reduces the sum-rate of the MSs on the cell edge.

Remark 4.6 is the consequence of both Theorem 4.3 and Theorem 4.5, which is numerically justified in Section 3.2. This remark reveals a problem in designing a conventional ORP scheme: specifically, how to achieve an optimal tradeoff between the coverage and sum-rate performance of the system. Therefore, a new design for the ORP scheme that further maximizes the coverage without reducing the sum-rate should be developed. Our attempt is presented in the next section.

4.3 Optimal trade-off between coverage and sum-rate performance

In this section, the use of multiple transmission slots to enhance both the maximum SINR of each user and the sum-rate performance is considered. In this scheme, the BS randomly generates a precoding matrix $\mathbf{\Phi} \in \mathbb{C}^{N_t \times (ND)}$:

$$\mathbf{\Phi} = \begin{bmatrix} \phi_{1,1}^{(1)} & \dots & \phi_{1,N}^{(1)} & \dots & \phi_{1,1}^{(D)} & \dots & \phi_{1,N}^{(D)} \\ \phi_{2,1}^{(1)} & \dots & \phi_{2,N}^{(1)} & \dots & \phi_{2,1}^{(D)} & \dots & \phi_{2,N}^{(D)} \\ \vdots & \vdots & \vdots & \vdots & \vdots & \vdots & \vdots \\ \phi_{N_t,1}^{(1)} & \dots & \phi_{N_t,N}^{(1)} & \dots & \phi_{N_t,1}^{(D)} & \dots & \phi_{N_t,N}^{(D)} \end{bmatrix},$$

where D is the number of transmission slots, and $\mathbf{\Phi}$ consists of ND orthonormal precoding vectors $\boldsymbol{\phi}_n^{(d)}$, which denote the nth precoding vector used in the time slot d, $n = 1, \dots, N$, $d = 1, \dots, D$, with the constraint $ND \leq N_t$. For each transmission slot, one cycle of the training and transmission phases occurs. In the training phase of the first cycle, N training signals are multiplied by the first group of N precoding vectors $\left\{\boldsymbol{\phi}_1^{(1)}, \boldsymbol{\phi}_2^{(1)}, \dots, \boldsymbol{\phi}_N^{(1)}\right\}$ before being sent to the MSs. Then, each MS computes N SINR values from the output of the MMSE receiver and determines the maximum value. The maximum SINR and the index of the effective beam of each MS are fed back to the BS. If an MS has a maximum SINR that is higher than γ, it is determined to be in coverage and can be selected for transmission. In the transmission phase, instead of randomly assigning a precoding vector to an MS, the BS uses the effective beam of the MS to precode the transmit signals. In the dth cycle, $d = 2, 3, \dots, D$, similar operations are performed with the dth precoder group $\left\{\boldsymbol{\phi}_1^{(d)}, \boldsymbol{\phi}_2^{(d)}, \dots, \boldsymbol{\phi}_N^{(d)}\right\}$.

We assume that an MS has a delay constraint of D transmission slots for a certain traffic type. In this case, D consecutive cycles of training and transmission phases can be considered to find the MS's effective beam within the delay constraint. Therefore, the maximum SINR can be searched for over ND beams. This implies that a larger D provides a higher chance for the maximum SINR to be larger than the SINR threshold γ, which increases the coverage probability. In the following subsection, we investigate both the optimal coverage probability and sum-rate of the ORP scheme with multiple precoder groups.

Remark 4.7. For transmissions of D multiple precoder groups over multiple time slots, the downlink coverage probability is given by

$$\mathcal{P}(\gamma, N) \approx 1 - \left(\sum_{k=1}^{N_r-\eta} \frac{1 - e^{-\frac{N}{\rho \xi_k}\gamma}}{\prod_{i=1, i\neq k}^{N_r-\eta} \left(1 - \frac{\xi_i}{\xi_k}\right)} \right)^{ND}. \tag{4.27}$$

Proof. At the receiver, the maximum SINR is selected not only from N beams but also from D transmission slots. In the dth slot, the SINR for the nth beam, $\boldsymbol{\phi}_n^{(d)}$, in the output of the MMSE receiver can be expressed as

$$\mathcal{X}_{n,\mathrm{MMSE}}^{(d)} = \left(\tilde{\boldsymbol{h}}_n^{(d)}\right)^H \left[\tilde{\boldsymbol{H}}_{-n}^{(d)} \left(\tilde{\boldsymbol{H}}_{-n}^{(d)}\right)^H + \frac{N}{\rho}\boldsymbol{I}\right]^{-1} \tilde{\boldsymbol{h}}_n^{(d)},$$

where $\tilde{\boldsymbol{h}}_n^{(d)}$ is the nth column of the matrix $\tilde{\boldsymbol{H}}^{(d)} = \boldsymbol{H}\left[\boldsymbol{\phi}_1^{(d)}, \boldsymbol{\phi}_2^{(d)}, \ldots, \boldsymbol{\phi}_N^{(d)}\right]$, and $\tilde{\boldsymbol{H}}_{-n}^{(d)}$ is obtained by removing the nth column of $\tilde{\boldsymbol{H}}^{(d)}$. In this scheme, the ND precoding vectors in $\boldsymbol{\Phi}$ are mutually orthogonal, and therefore, $\boldsymbol{H}\boldsymbol{\phi}_n^{(d)}$, $n = 1, \ldots, N$, and $d = 1, \ldots, D$, are independent. As a result, the ND values of the SINR are independent, which yields

$$\mathcal{P}(\gamma, N) = 1 - \mathbf{P}\left\{ \max_{\substack{n=1,\ldots,N \\ d=1,\ldots,D}} \mathcal{X}_{n,\mathrm{MMSE}}^{(d)} \leq \gamma \right\} = 1 - \left[F_{\mathcal{X}_{max,\mathrm{MMSE}}}(\gamma)\right]^D. \tag{4.28}$$

From (4.17) and (4.28), we obtain $\mathcal{P}(\gamma, N)$ in (4.27), and the proof is complete. □

By comparing the results in Remark 4.7 with those in Remark 4.2, we observe that the M-ORP scheme employing multiple transmission slots can lead to a significant improvement in terms of coverage. The optimal coverage performance of the M-ORP scheme is achieved when the maximum number of transmission slots is exploited. In the case that $D = \frac{N_t}{N}$ satisfies the delay constraint, the coverage probability is given by

$$\mathcal{P}(\gamma, N) \approx 1 - \left(\sum_{k=1}^{N_r-\eta} \frac{1 - e^{-\frac{N}{\rho\xi_k}\gamma}}{\prod_{i=1, i\neq k}^{N_r-\eta} \left(1 - \frac{\xi_i}{\xi_k}\right)} \right)^{N_t}.$$

In a massive MIMO system with a large number of transmit antennas, we can achieve $\mathcal{P}(\gamma, N) \longrightarrow 1$ if a large delay is allowed. Note that there is no improvement in terms of the average sum-rate of each transmission slot. However, an M-ORP scheme with more transmission slots allows the BS to have a higher coverage probability without sacrificing the sum-rate performance. As a result, the tradeoff between coverage and sum-rate performance is further optimized. The simulation results presented in the next section will justify this conclusion numerically.

4.4 Numerical results

In this section, we provide numerical results to evaluate the coverage and sum-rate performance of the ORP scheme with MMSE receivers. Similar to simulations in Chapter 3, a precoding matrix with orthonormal precoding vectors is created by computing an orthonormal basis for the column space of a randomly generated matrix. Furthermore, the coefficients of the channel matrix are randomly generated as $\mathcal{CN}(0, 1)$ random variables and fixed over D time slots. We consider $N_t \in \{32, 240\}$ transmit antennas at the BS and $N_r = 16$ receive antennas at the MSs with MMSE receivers, and the number of precoding

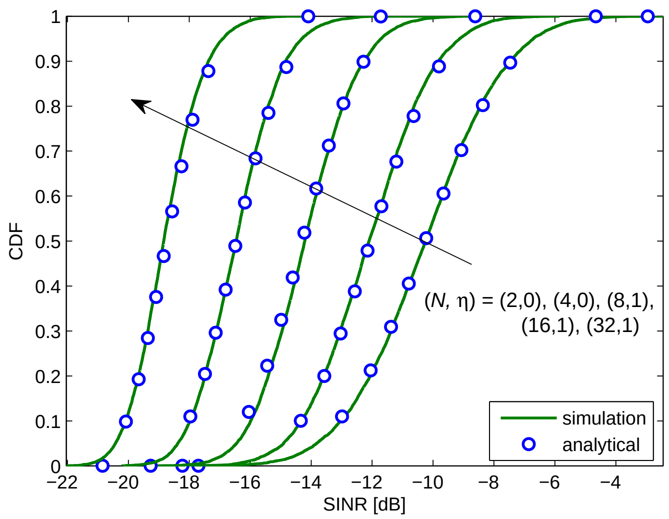

FIG. 4.1. Comparison between analytical and simulation CDFs of the maximum SINR for $\rho = -20$ dB, $(\varepsilon_t, \varepsilon_r) = (0.1, 0.9)$, $N_t = 32$, $N_r = 16$, and $N \in \{2, 4, 8, 16, 32\}$.

vectors is chosen such that $N \in [1, N_t]$. In this study, an exponential correlation model is assumed, because it is physically reasonable in the sense that the correlation decreases with the distance between antennas, and it also matches some realistic physical configurations [34]. In this correlation model, the correlation matrix $\boldsymbol{R}(\varepsilon)$ is defined as

$$\boldsymbol{R}(\varepsilon) = \begin{bmatrix} 1 & \varepsilon & \varepsilon^2 & \dots & \varepsilon^{M-1} \\ \varepsilon & 1 & \varepsilon & \dots & \varepsilon^{M-2} \\ \vdots & \vdots & \vdots & \ddots & \vdots \\ \varepsilon^{M-1} & \varepsilon^{M-2} & \varepsilon^{M-3} & \dots & 1 \end{bmatrix},$$

where (ε, M) is (ε_t, N_t) for $\boldsymbol{R}_t(\varepsilon_t)$ and is (ε_r, N_r) for $\boldsymbol{R}_r(\varepsilon_r)$. To generate a near semi-highly correlated channel, we assume that the correlation coefficients at the BS and MS are $\varepsilon_t = 0.1$ and $\varepsilon_r = 0.9$, respectively. Furthermore, to account for the large propagation loss at the cell edge of mmWave communication systems, we assume that the average SNR for cell-edge MSs is as low as $\rho = -20$ dB.

First, we validate the accuracy of the approximate analytical CDF of the maximum SINR,

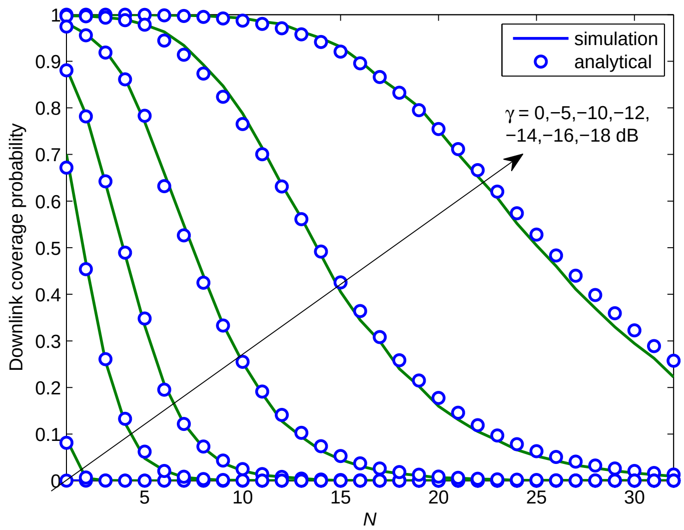

FIG. 4.2. Downlink coverage probability versus the number of precoding vectors N of the ORP scheme with MMSE receivers for $\rho = -20$ dB, $(\varepsilon_t, \varepsilon_r) = (0.1, 0.9)$, $N_t = 32$, $N_r = 16$, and $\gamma \in \{-18, -16, -14, -12, -10, -5, 0\}$ dB.

given in Theorem 4.1, by comparing it to the simulation results. It is clear that a larger N leads to a larger CDF value for the maximum SINR. Furthermore, it is shown that by adjusting η slightly, the approximate analytical results in (4.16) match the simulation results well. Specifically, $\eta = 0$ should be chosen for a small N, while $\eta = 1$ results in more accurate analytical results for large N values. In the subsequent simulations, we will use this adjustment of η to obtain an accurate approximation of the analytical results.

Fig. 4.2 shows the coverage behavior of the ORP scheme with MMSE receivers with respect to the number of precoding vectors N for $N_t = 32$, $N_r = 16$, $(\varepsilon_t, \varepsilon_r) = (0.1, 0.9)$, and different γ values. In this figure, it can be seen that the analytical results of the downlink coverage probability based on the approximation (4.18) in Remark 4.2 is close to the simulation results. It is clear that the coverage probability decreases with N and that for each γ, the optimal number of precoding vectors is one, i.e., $N^\star = 1$.

For further illustration of the coverage performance improvement provided by the MMSE receivers, Fig. 4.3 compares the ORP scheme with MMSE receivers (ORP-MMSE) to

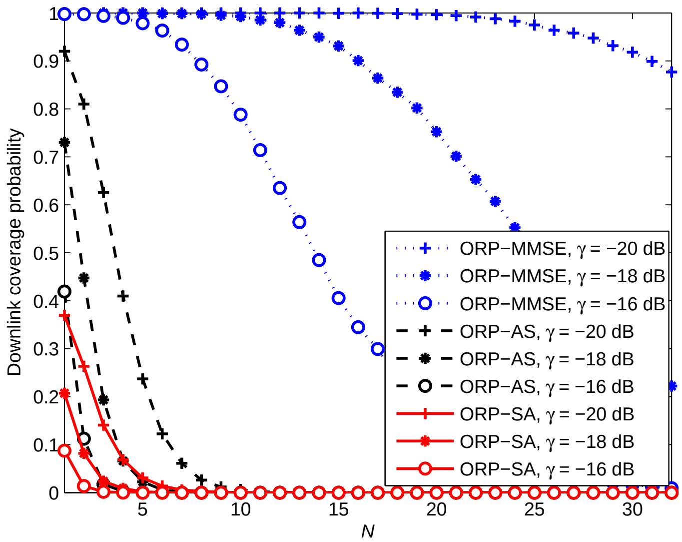

FIG. 4.3. Comparison among coverage performances provided by single antenna (SA), antenna selection (AS), and MMSE receivers with $\rho = -20$ dB, $(\varepsilon_t, \varepsilon_r) = (0.1, 0.9)$, $\gamma \in \{-16, -18, -20\}$ dB, $N_r \in \{1, 16\}$, and $N_t = 32$.

the ORP-AS and ORP-SA schemes, which were analyzed in [27], with $N_r = 16$ for both ORP-AS and ORP-MMSE schemes. In this simulation, we still assume $N_t = 32$, $(\varepsilon_t, \varepsilon_r) = (0.1, 0.9)$, and $\gamma \in \{-16, -18, -20\}$ dB. It is clear that the ORP-MMSE scheme achieves considerably higher coverage probabilities than the ORP-SA and ORP-AS schemes.

Fig. 4.4 compares the sum-rate of the ORP-MMSE scheme with those of the ORP-SA and ORP-AS schemes. In this simulation, the sum-rate is computed as in (4.26). Firstly, it is clear that the sum-rate of the ORP-MMSE scheme is an increasing function of N and is optimized as $N^\star = N_t$, which is stated in Theorem 4.5. Secondly, it is also clear that the ORP-MMSE scheme achieves a considerably high sum-rate compared to the two other schemes. Furthermore, the performance gain provided by the ORP-MMSE scheme is much larger than that provided by the ORP-AS scheme as a larger number of receive antennas are employed.

Finally, Fig. 4.5 and Fig. 4.6 show the advantage of the M-ORP scheme in the optimization of coverage–sum-rate tradeoff and in the comparison with STC scheme. In Fig. 4.5, it is

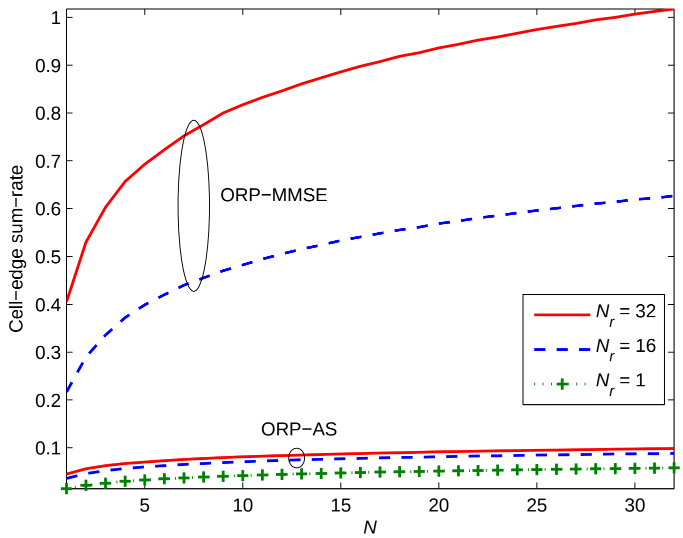

FIG. 4.4. Comparison among sum-rates provided by single antenna (SA), antenna selection (AS), and MMSE receivers with $\rho = -20$ dB, $(\varepsilon_t, \varepsilon_r) = (0.1, 0.9)$, $N_r \in \{1, 16, 32\}$, and $N_t = 32$.

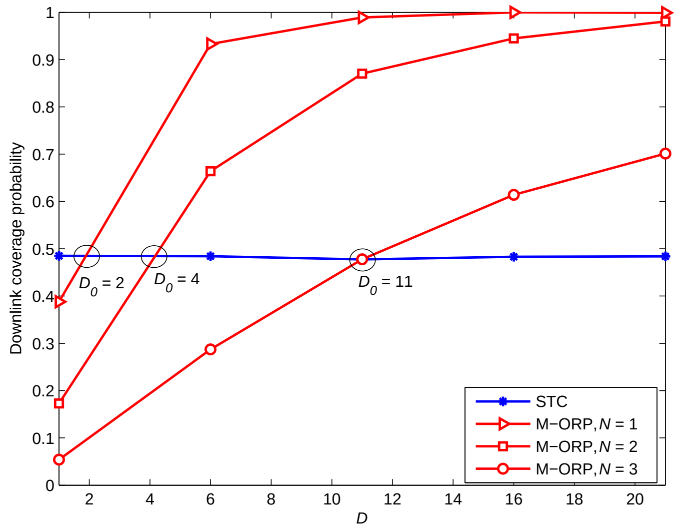

FIG. 4.5. Comparison of the STC and ORP schemes for $N_t = 64$, $N_r = 1$, $N \in \{1, 2, 3\}$, and $\gamma = \rho = -2$ dB.

shown that as D increases, the coverage probability of the ORP scheme increases. In contrast, the STC scheme has almost constant coverage probability because the channel is assumed to be fixed over D time slots. Meanwhile, in Fig. 4.6, it is clear that the M-ORP scheme significantly improves the coverage performance of the original ORP scheme.

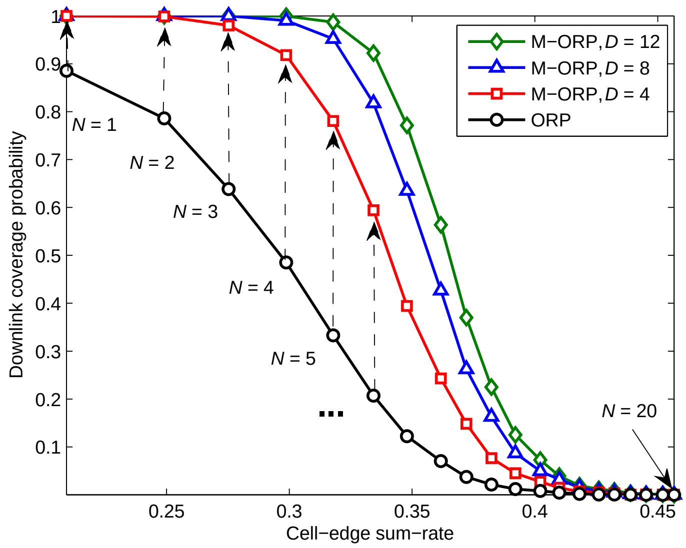

FIG. 4.6. Coverage–sum-rate tradeoff improvement of the M-ORP scheme with $\rho = -20$ dB, $\gamma = -12$ dB, $(\varepsilon_t, \varepsilon_r) = (0.1, 0.9), D = \{1, 4, 8, 12\}, N = \{1, 2, \dots, 20\}$, $N_t = 240$, and $N_r = 16$.

For example, with $N = 5$ precoding vectors, the ORP scheme achieves an approximate coverage probability of 0.3, while the coverage probabilities for the M-ORP scheme are close to 0.8, 0.95, and 1 for $D = 4, 8$, and 12, respectively. Therefore, the M-ORP scheme is advantageous in optimizing the coverage–sum-rate tradeoff. In particular, to cover an MS with a coverage probability close to 0.9, the required sum-rate for the MSs on the cell edge is only about 0.2. However, a sum-rate of nearly 0.35 can be achieved with the same coverage probability when the M-ORP scheme is employed with $D = 12$ transmission slots.

Chapter 5

Conclusions

In this thesis, the cell coverage extension problem in massive MIMO systems was considered. As one eligible solution for this problem, we proposed the use of the ORP scheme, where the transmit signals are precoded by the orthonormal precoding vectors. The analytical closed-form expression of the coverage probability was derived. It was shown that to reduce the deleterious effects of interference from the ineffective beams and to achieve optimal coverage performance, the use of a small number of precoding vectors is desirable.

To further extend the coverage, we investigated the ORP-AS, ORP-MMSE, and M-ORP schemes, which can significantly improve the coverage performance. The analytical results were confirmed through numerical results, which proved the accuracy of our derived expressions. We also consider the ORP scheme in mmWave massive MIMO systems. To address more practical communication environments, future studies could consider both the coverage and sum-rate performance of the ORP scheme with respect to the effects of inter-cell interference.

Bibliography

[1] H. Q. Ngo, E. G. Larsson, and T. L. Marzetta, "Energy and spectral efficiency of very large multiuser MIMO systems," *IEEE Trans. Commun.*, vol. 61, no. 4, pp. 1436–1449, 2013.

[2] T. L. Marzetta, "Noncooperative cellular wireless with unlimited numbers of base station antennas," *IEEE Trans. Wireless Commun.*, vol. 9, no. 11, pp. 3590–3600, 2010.

[3] A. L. Swindlehurst, E. Ayanoglu, P. Heydari, and F. Capolino, "Millimeter-wave massive MIMO: The next wireless revolution?" *IEEE Commun. Mag.*, vol. 52, no. 9, pp. 56–62, 2014.

[4] Y.-G. Lim, C.-B. Chae, and G. Caire, "Performance analysis of massive MIMO for cell-boundary users," *IEEE Trans. Wireless Commun.*, vol. 14, no. 12, pp. 6827–6842, 2015.

[5] L. Collin, O. Berder, P. Rostaing, and G. Burel, "Optimal minimum distance-based precoder for MIMO spatial multiplexing systems," *IEEE Trans. Signal Process.*, vol. 52, no. 3, pp. 617–627, 2004.

[6] N. D. Sidiropoulos, T. N. Davidson, and Z.-Q. Luo, "Transmit beamforming for physical-layer multicasting," *IEEE Trans. Signal Process.*, vol. 54, no. 6, pp. 2239–2251, 2006.

[7] C.-B. Chae and R. W. Heath Jr, "On the optimality of linear multiuser MIMO beamforming for a two-user two-input multiple-output broadcast system," *IEEE Signal Process. Let.*, vol. 16, no. 2, pp. 117–120, 2009.

[8] D. J. Love and R. W. Heath, "Limited feedback unitary precoding for spatial multiplexing systems," *IEEE Trans. Inf. Theory*, vol. 51, no. 8, pp. 2967–2976, 2005.

[9] J. Choi, D. J. Love, and P. Bidigare, "Downlink training techniques for FDD massive MIMO systems: Open-loop and closed-loop training with memory," *IEEE J. Sel. Topics in Signal Process.*, vol. 8, no. 5, pp. 802–814, 2014.

[10] Z. W. Z. Gao, L. Dai and S. Chen, "Spatially common sparsity based adaptive channel estimation and feedback for FDD massive MIMO," *IEEE Trans. Signal Process.*, vol. 63, no. 23, pp. 6169–6183, 2015.

[11] X. Rao and V. K. Lau, "Distributed compressive CSIT estimation and feedback for FDD multi-user massive MIMO systems," *IEEE Trans. Signal Process.*, vol. 62, no. 12, pp. 3261–3271, 2014.

[12] K. Huang, J. G. Andrews, and R. W. Heath Jr, "Performance of orthogonal beamforming for SDMA with limited feedback," *IEEE Trans. Veh. Tech.*, vol. 58, no. 1, pp. 152–164, 2009.

[13] M. Sharif and B. Hassibi, "On the capacity of MIMO broadcast channels with partial side information," *IEEE Trans. Inf. Theory.*, vol. 51, no. 2, pp. 506–522, 2005.

[14] T. Obara, S. Suyama, J. Shen, and Y. Okumura, "Joint fixed beamforming and eigenmode precoding for super high bit rate massive MIMO systems using higher frequency

bands," in *IEEE 25th Annual Int. Symposium on Personal, Indoor, and Mobile Radio Commun. (PIMRC).* IEEE, 2014, pp. 607–611.

[15] J. Nam, J.-Y. Ahn, A. Adhikary, and G. Caire, "Joint spatial division and multiplexing: Realizing massive MIMO gains with limited channel state information," in *IEEE 46th Annual Conf. Inf. Sciences and Systems (CISS).* IEEE, 2012, pp. 1–6.

[16] I.-H. Lee and D. Kim, "Coverage extension and power allocation in dual-hop space–time transmission with multiple antennas in each node," *IEEE Trans. Veh. Technol.*, vol. 56, no. 6, pp. 3524–3532, 2007.

[17] C.-J. Chen and L.-C. Wang, "Enhancing coverage and capacity for multiuser MIMO systems by utilizing scheduling," *IEEE Trans. Wireless Commun.*, vol. 5, no. 5, pp. 1148–1157, 2006.

[18] H. S. Dhillon, M. Kountouris, and J. G. Andrews, "Downlink coverage probability in MIMO HetNets," in *Proc. 46th Annu. Asilomar Conf. Signals, Syst., Comput.* IEEE, 2012, pp. 683–687.

[19] A. K. Gupta, H. S. Dhillon, S. Vishwanath, and J. G. Andrews, "Downlink coverage probability in MIMO HetNets with flexible cell selection," in *IEEE GLOBECOM*, 2014, pp. 1534–1539.

[20] T. Bai and R. W. Heath Jr, "Asymptotic coverage probability and rate in massive MIMO networks," *arXiv preprint arXiv:1305.2233*, 2013.

[21] S. Jin, J. Wang, Q. Sun, M. Matthaiou, and X. Gao, "Cell Coverage Optimization for the Multicell Massive MIMO Uplink," *IEEE Trans. Veh. Technol.*, vol. 64, no. 12, pp. 5713–5727, 2015.

[22] H. D. Nguyen, R. Zhang, and H. T. Hui, "Effect of receive spatial diversity on the degrees of freedom region in multi-cell random beamforming," in *Proc. 2013 IEEE Wireless Commun. and Networking Conf.*, pp. 3028–3033.

[23] ——, "Multi-cell random beamforming: Achievable rate and degrees of freedom region," *IEEE Trans. Signal Process.*, vol. 61, no. 14, pp. 3532–3544, 2013.

[24] P. Viswanath, D. N. Tse, and R. Laroia, "Opportunistic beamforming using dumb antennas," *IEEE Trans. Inf. Theory*, vol. 48, no. 6, pp. 1277–1294, 2002.

[25] Z. Pi and F. Khan, "An introduction to millimeter-wave mobile broadband systems," *IEEE Commun. Mag.*, vol. 49, no. 6, pp. 101–107, 2011.

[26] O. El Ayach, S. Rajagopal, S. Abu-Surra, Z. Pi, and R. W. Heath, "Spatially sparse precoding in millimeter wave MIMO systems," *IEEE Trans. Wireless Commun.*, vol. 13, no. 3, pp. 1499–1513, 2014.

[27] T. N. Nguyen and K. Lee, "Cell Coverage Extension With Orthogonal Random Precoding for Massive MIMO Systems," *IEEE Access*, vol. 5, pp. 5410–5424, 2017.

[28] ——, "Coverage and Cell-edge Sum-rate Analysis of mmWave Massive MIMO Systems with the ORP Scheme and MMSE Receiver," *submitted to IEEE Trans. Signal Process.*, 2017.

[29] 3GPP TS 36.211 V10.9.0, "Evolved Universal Terrestrial Radio Access (EUTRA); Physical channels and modulation," Mar. 2013.

[30] 3GPP TS 36.331 V10.20.0, "Evolved Universal Terrestrial Radio Access (EUTRA); Radio resource Control (RRC) protocol specification," Dec. 2016.

[31] Z. Gao, L. Dai, D. Mi, Z. Wang, M. A. Imran, and M. Z. Shakir, "MmWave massive-MIMO-based wireless backhaul for the 5G ultra-dense network," *IEEE Wireless Commun.*, vol. 22, no. 5, pp. 13–21, 2015.

[32] J. Choi, "On coding and beamforming for large antenna arrays in mm-wave systems," *IEEE Wireless Commun. Lett.*, vol. 3, no. 2, pp. 193–196, 2014.

[33] N. Kim, Y. Lee, and H. Park, "Performance analysis of MIMO system with linear MMSE receiver," *IEEE Trans. Wireless Commun.*, vol. 7, no. 11, pp. 4474–4478, 2008.

[34] S. L. Loyka, "Channel capacity of MIMO architecture using the exponential correlation matrix," *IEEE Commun. Lett.*, vol. 5, no. 9, pp. 369–371, 2001.

[35] F. Qeadan, T. J. Kozubowski, and A. K. Panorska, "The Joint Distribution of the Sum and the Maximum of IID Exponential Random Variables," *Comm. Statist. Theory Methods*, vol. 41, no. 3, pp. 544–569, 2012.

[36] A. Adhikary, J. Nam, J.-Y. Ahn, and G. Caire, "Joint spatial division and multiplexing—the large-scale array regime," *IEEE Trans. Inf. Theory*, vol. 59, no. 10, pp. 6441–6463, 2013.

[37] D. Hammarwall, M. Bengtsson, and B. Ottersten, "Acquiring partial CSI for spatially selective transmission by instantaneous channel norm feedback," *IEEE Trans. on Signal Process.*, vol. 56, no. 3, pp. 1188–1204, 2008.

Appendix A

.1 Proof of Theorem 3.1

Let $A_n = \left|\boldsymbol{h}^T \boldsymbol{\phi}_n\right|^2$, and $B_n = \sum_{i \neq n}^{N} \left|\boldsymbol{h}^T \boldsymbol{\phi}_i\right|^2$. We rewrite (3.2) as $\mathcal{X}_n = \frac{A_n}{N/\rho + B_n}$. Let $A_{max} = \max\limits_{n=1,\ldots,N} A_n$, and $B_{min} = \min\limits_{n=1,\ldots,N} \sum_{i \neq n}^{N} B_n$. We can write

$$\mathcal{X}_{max} = \frac{A_{max}}{N/\rho + B_{min}}, \tag{1}$$

where we have $A_{max} \leq \frac{B_{min}}{N-1}$. From Definition 2.1 and (1), the downlink coverage probability can be expressed as

$$\begin{aligned} \mathcal{P}(\gamma, N) &= \mathbf{P}\left\{\mathcal{X}_{max} > \gamma\right\} = \mathbf{P}\left\{A_{max} > \gamma \left(\frac{N}{\rho} + B_{min}\right)\right\} \\ &= \int_0^{\infty} \int_{\gamma\left(\frac{N}{\rho}+b\right)}^{\infty} f_{A_{max},B_{min}}(a, b) da db. \end{aligned} \tag{2}$$

First, we derive the joint distribution of A_{max} and B_{min}, i.e., $f_{A_{max},B_{min}}(a, b)$. Because $\mathbf{\Phi}$ is composed of orthonormal vectors and the coefficients of $\boldsymbol{h}^T$ are random variables of $\mathcal{CN}(0, 1)$, $\boldsymbol{h}^T \boldsymbol{\phi}_n$ has the same distribution. Therefore, A_n becomes a central chi-square random variable of two degrees of freedom with mean $\epsilon^2 = 1$, i.e., $A_n \sim \chi^2(1)$. The probability density function (PDF) and the CDF of A_n are given by

$$\begin{aligned} f_{A_n}(a) &= e^{-a}, \\ F_{A_n}(a) &= 1 - e^{-a}, \end{aligned} \tag{3}$$

respectively. Because $A_i = \left|\boldsymbol{h}^T \boldsymbol{\phi}_i\right|^2$ and $A_j = \left|\boldsymbol{h}^T \boldsymbol{\phi}_j\right|^2$ are independent for all i and j, we have

$$F_{A_{max}}(a) = \mathbf{P}\left\{A_{max} \le a\right\} = \left[\mathbf{P}\left\{A_n \le a\right\}\right]^N = \left[F_{A_n}(a)\right]^N = (1 - e^{-a})^N,$$

which leads to the PDF of A_{max}:

$$f_{A_{max}}(a) = \frac{d}{da} F_{A_{max}}(a) = N(1 - e^{-a})^{N-1} e^{-a}. \tag{4}$$

Let $S = \sum_{n=1}^{N} \left|\boldsymbol{h}^T \boldsymbol{\phi}_n\right|^2 = \sum_{n=1}^{N} A_n = A_{max} + B_{min}$. We observe that

$$\begin{aligned} F_{B_{min}|A_{max}}(b|a) &= \mathbf{P}\left\{B_{min} \le b | A_{max} = a\right\} = \mathbf{P}\left\{A_{max} + B_{min} \le a + b | A_{max} = a\right\} \\ &= \mathbf{P}\left\{S \le a + b | A_{max} = a\right\} = F_{S|A_{max}}(s|a), \end{aligned} \tag{5}$$

where $s = a + b$. The PDF of S conditioned on A_{max} is expressed as [35]

$$f_{S|A_{max}}(s|a) = \frac{s^{N-2} e^{-(s-a)}}{N!\,(1 - e^{-a})^{N-1}} h_N\left(\frac{a}{s}\right), \tag{6}$$

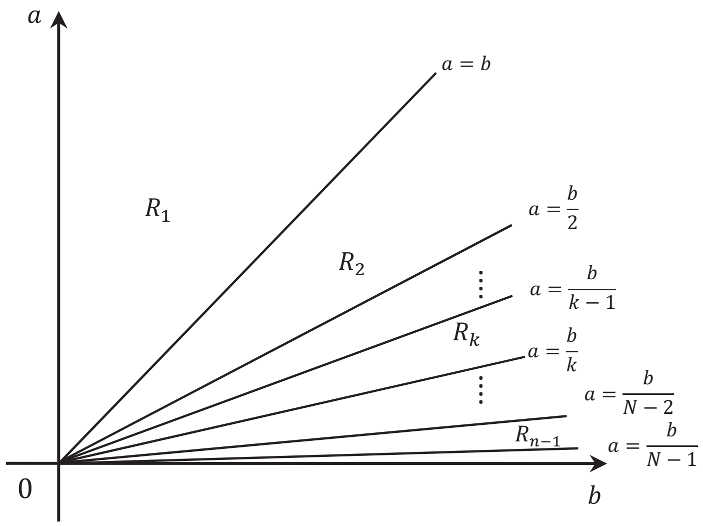

FIG. 1. Feasible regions of the joint PDF of A_{max} and B_{min}.

where

$$h_N\left(\frac{a}{s}\right) = \begin{cases} N(N-1)\sum_{t=1}^{k}\binom{N-1}{t-1}(-1)^{t+1}\left(1-t\frac{a}{s}\right)^{N-2}, & \frac{1}{k+1} \le \frac{a}{s} \le \frac{1}{k},\ k=1,\dots,N-1 \\ 0, & \text{otherwise.} \end{cases} \tag{7}$$

From (5)–(7), it is clear that the distribution of B_{min} conditioned on A_{max} depends on the regions to which point (a, b) belongs. We define regions R_k, $k = 1, \dots, N-1$, to be

$$R_1 = \left\{(a,b) \in \mathbb{R}_+^2 : a \ge b\right\}, \tag{8}$$

$$R_k = \left\{(a,b) \in \mathbb{R}_+^2 : \frac{b}{k} \le a \le \frac{b}{k-1}\right\},\ k = 2,\dots,N-1. \tag{9}$$

Fig. 1 illustrates the regions R_k, each of which corresponds to a different form of $h_N\left(\frac{a}{s}\right)$ in (7). We can then obtain the PDF of B_{min} conditioned on A_{max} in the form of

$$f_{B_{min}|A_{max}}(b|a) = \frac{e^{-b}}{(1-e^{-a})^{N-1}(N-2)!}\sum_{t=1}^{k}\binom{N-1}{t-1}(-1)^{t+1}[b-(t-1)a]^{N-2},$$

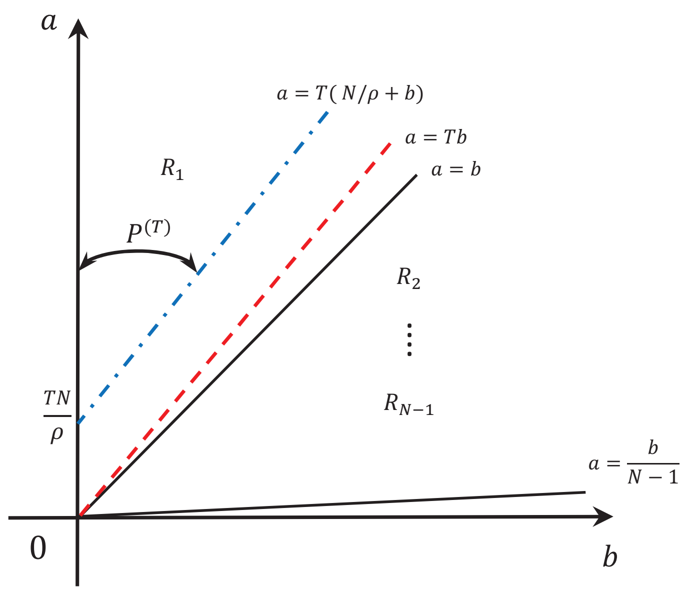

FIG. 2. Feasible regions for determining $\mathcal{P}(\gamma, N)$ for $\gamma \geq 1$.

$$(a, b) \in R_k,\ k = 1, \ldots, N-1, \tag{10}$$

with the constraint $0 \leq b \leq (N-1)a$. From (4) and (10), the joint PDF of A_{max} and B_{min} is expressed as

$$\begin{aligned} f_{A_{max},B_{min}}(a, b) &= f_{B_{min}|A_{max}}(b|a) f_{A_{max}}(a) \\ &= \frac{N}{(N-2)!} e^{-(a+b)} \sum_{t=1}^{k} \binom{N-1}{t-1} (-1)^{t+1} [b - (t-1)a]^{N-2}, (a, b) \in R_k. \end{aligned} \tag{11}$$

For simplicity, we denote $f_k(a, b) = f_{A_{max},B_{min}}(a, b)$, $(a, b) \in R_k$. We now evaluate the integral in (2) by considering two cases:

- **Case 1:** $\gamma \geq 1$

From (2) and Fig. 2, the downlink coverage probability in this case can be expressed as

$$\mathcal{P}(\gamma, N) = \int_0^\infty \int_{\gamma\left(\frac{N}{\rho}+b\right)}^\infty f_1(a, b) da db.$$

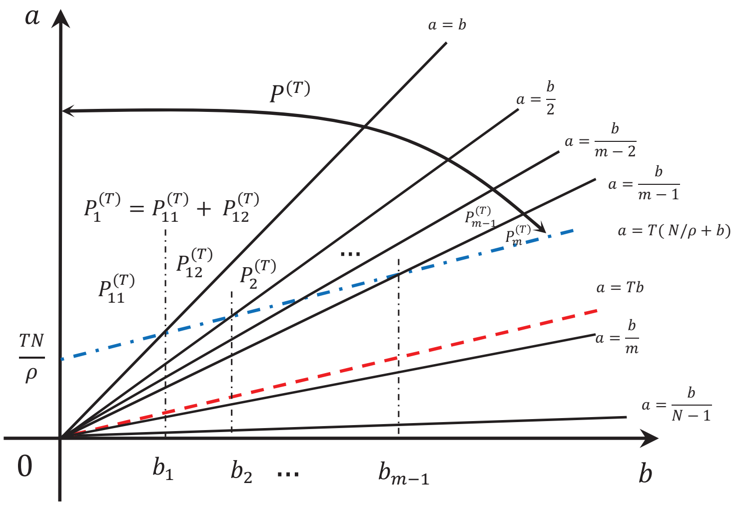

FIG. 3. Feasible regions for determining $\mathcal{P}(\gamma, N)$ for $0 < \gamma < 1$.

In R_1, the joint distribution of A_{max} and B_{min} in (11) can be rewritten as

$$f_1(a,b) = \frac{N}{(N-2)!} e^{-(a+b)} b^{N-2}. \tag{12}$$

Hence, $\mathcal{P}(\gamma, N)$ is expressed as

$$\mathcal{P}(\gamma, N) = \frac{N}{(N-2)!} \int_0^{\infty} \int_{\gamma\left(\frac{N}{\rho}+b\right)}^{\infty} e^{-(a+b)} b^{N-2} da db = \frac{N}{N-1} e^{-\gamma N/\rho} \int_0^{\infty} e^{-(\gamma+1)b} b^{N-2} db.$$

By applying the partial integration, we obtain

$$\mathcal{P}(\gamma, N) = \frac{N}{(\gamma+1)^{N-1}} e^{-\gamma N/\rho}. \tag{13}$$

- **Case 2:** $0 < \gamma < 1$

From (2) and Fig. 3, the downlink coverage probability in this case can be expressed as

$$\begin{aligned}\mathcal{P}(\gamma, N) &= \mathcal{P}(\gamma, N)_1 + \mathcal{P}(\gamma, N)_2 + \ldots + \mathcal{P}(\gamma, N)_{m-1} + \mathcal{P}(\gamma, N)_m \\ &= \mathcal{P}(\gamma, N)_1 + \sum_{i=2}^{m-1} \mathcal{P}(\gamma, N)_i + \mathcal{P}(\gamma, N)_m, \end{aligned} \tag{14}$$

where

$$\mathcal{P}(\gamma,N)_1=\underbrace{\int_0^{b_1}\int_{\gamma\left(\frac{N}{\rho}+b\right)}^{\infty} f_1(a,b)dadb}_{:=\mathcal{P}(\gamma,N)_{11}}+\underbrace{\int_{b_1}^{\infty}\int_{b}^{\infty} f_1(a,b)dadb}_{:=\mathcal{P}(\gamma,N)_{12}}, \tag{15}$$

$$\mathcal{P}(\gamma,N)_k=\underbrace{\int_{b_{k-1}}^{b_k}\int_{\gamma\left(\frac{N}{\rho}+b\right)}^{\frac{b}{k-1}} f_k(a,b)dadb}_{:=\mathcal{P}(\gamma,N)_{k1}}+\underbrace{\int_{b_k}^{\infty}\int_{\frac{b}{k}}^{\frac{b}{k-1}} f_k(a,b)dadb}_{:=\mathcal{P}(\gamma,N)_{k2}},\ k=2,\ldots,m-1, \tag{16}$$

$$\mathcal{P}(\gamma,N)_m=\int_{b_{m-1}}^{\infty}\int_{\gamma\left(\frac{N}{\rho}+b\right)}^{\frac{b}{m-1}} f_m(a,b)dadb,\ m=\left\lceil\frac{1}{\gamma}\right\rceil, \tag{17}$$

and $b_k,\ k=1,\ldots,N-1$, is the intersection point between the two lines $a=\gamma\left(\frac{N}{\rho}+b\right)$ and $a=\frac{b}{k}$, as given by (3.1). Inserting (12) into (15), we obtain

$$\mathcal{P}(\gamma,N)_1=\frac{N}{(N-2)!}\left[e^{-\frac{\gamma N}{\rho}}\underbrace{\int_0^{b_1} e^{-(\gamma+1)b}b^{N-2}db}_{:=C_1}+\underbrace{\int_{b_1}^{\infty} e^{-2b}b^{N-2}db}_{:=C_2}\right]. \tag{18}$$

Using the lower incomplete Gamma function for an integer n, which is C_1 and C_2 can be expressed as

$$\begin{aligned}C_1&=\int_0^{b_1} e^{-(\gamma+1)b}b^{N-2}db=\int_0^{\infty} e^{-(\gamma+1)b}b^{N-2}db-\int_{b_1}^{\infty} e^{-(\gamma+1)b}b^{N-2}db\\&=\frac{(N-2)!}{(\gamma+1)^{N-1}}\left(1-e^{-(\gamma+1)b_1}\sum_{l=0}^{N-2}\frac{(\gamma+1)^l b_1^l}{l!}\right),\\C_2&=\int_{b_1}^{\infty} e^{-2b}b^{N-2}db=\frac{(N-2)!}{2^{N-1}}e^{-2b_1}\sum_{l=0}^{N-2}\frac{2^l b_1^l}{l!},\end{aligned}$$

which are the expressions in (3.8) and (3.9) in Appendix **??**. Combining (3.8), (3.9), and (18), we obtain

$$\mathcal{P}(\gamma,N)_1=\frac{N}{(N-2)!}\left(e^{-\frac{\gamma N}{\rho}}C_1+C_2\right), \tag{19}$$

which is given by (3.4) in Theorem 3.1.

We next evaluate $\mathcal{P}(\gamma, N)_k$ in (16) by separately considering $\mathcal{P}(\gamma, N)_{k1}$ and $\mathcal{P}(\gamma, N)_{k2}$. Inserting (11) into (16) yields

$$\mathcal{P}(\gamma, N)_{k1} = \frac{N}{(N-2)!} \sum_{t=1}^{k} \binom{N-1}{t-1} (-1)^{t+1} \underbrace{\int_{b_{k-1}}^{b_k} \int_{\gamma\left(\frac{N}{\rho}+b\right)}^{\frac{b}{k-1}} e^{-(a+b)} \left[b-(t-1)a\right]^{N-2} dadb}_{:=I}. \tag{20}$$

Using the binomial expansion, we have $[b-(t-1)a]^{N-2} = \sum_{i=0}^{N-2} \binom{N-2}{i} b^{N-i-2} (1-t)^i a^i$. Hence, I in (20) becomes

$$I = \sum_{i=0}^{N-2} \binom{N-2}{i} (1-t)^i \underbrace{\int_{b_{k-1}}^{b_k} \underbrace{\int_{\gamma\left(\frac{N}{\rho}+b\right)}^{\frac{b}{k-1}} e^{-a} a^i da}_{:=I_{ia}} \, e^{-b} b^{N-i-2} db}_{:=I_i}. \tag{21}$$

Exploiting the definition of incomplete Gamma function, we obtain

$$I_{ia} = i! \sum_{l=0}^{i} \left(e^{-\gamma\left(\frac{N}{\rho}+b\right)} \frac{\gamma^l \left(\frac{N}{\rho}+b\right)^l}{l!} - e^{-\frac{b}{k-1}} \frac{b^l}{(k-1)^l l!} \right).$$

Hence,

$$I_i = i! \sum_{l=0}^{i} \left(e^{-\frac{\gamma N}{\rho}} \frac{\gamma^l}{l!} D_1 - \frac{1}{(k-1)^l l!} D_2 \right). \tag{22}$$

Through steps similar to those for the derivations of C_1 and C_2, we can obtain the expressions for D_1 and D_2 as given in (3.10) and (3.11). From (20)–(22), and $\xi_p(\cdot)$ in (3.7), $\mathcal{P}(\gamma, N)_{k1}$ can be rewritten as

$$\mathcal{P}(\gamma, N)_{k1} = \xi_k \left(e^{-\frac{\gamma N}{\rho}} \frac{\gamma^l}{l!} D_1 - \frac{1}{(k-1)^l l!} D_2 \right). \tag{23}$$

In a similar manner, the expressions of $\mathcal{P}(\gamma, N)_{k2}$ and $\mathcal{P}(\gamma, N)_m$ can also be derived as

$$\mathcal{P}(\gamma, N)_{k2} = \xi_k \left(e^{-\frac{\gamma N}{\rho}} \frac{\gamma^l}{l!} E_1 - \frac{1}{(k-1)^l l!} E_2 \right), \tag{24}$$

$$\mathcal{P}(\gamma, N)_m = \xi_m \left(e^{-\frac{\gamma N}{\rho}} \frac{\gamma^l}{l!} F_1 - \frac{1}{(m-1)^l l!} F_2 \right), \tag{25}$$

where E_1, E_2, F_1, and F_2 are given in (3.12)–(3.15) in Theorem 3.1. Finally, Theorem 3.1 is proved by combining (14), (19), and (23)–(25).

.2 Prove of Remark 3.3

Since $\frac{N}{(\gamma+1)^{N-1}} \leq \frac{N}{2^{N-1}} \leq 1$ and $e^{-\frac{\gamma N}{\rho}} \leq e^{-\frac{\gamma}{\rho}}$ as $\gamma \geq 1, N \geq 1$,, we obtain

$$\mathcal{P}(\gamma, N) = \frac{N}{(\gamma+1)^{N-1}} e^{-\frac{\gamma N}{\rho}} \leq e^{-\frac{\gamma}{\rho}}, \ \gamma \geq 1, N \geq 1, \tag{26}$$

where the equality occurs for $N = 1$. Therefore, we can conclude that when $\gamma \geq 1$, $N^\star = 1$.

We now prove that $\mathcal{P}(\gamma, N)$ with $\gamma \geq 1$ is a decreasing function of N. We observe that

$$\frac{\partial \mathcal{P}(\gamma, N)}{\partial N} = -\frac{e^{-\frac{\gamma N}{\rho}}}{(\gamma+1)^{N-1}} \left(\frac{\gamma N}{\rho} + N \log(\gamma+1) - 1 \right) < 0, \ \gamma \geq 1, N \geq 2. \tag{27}$$

Hence, $\mathcal{P}(\gamma, N)$ is a decreasing function of N on the range $[2; \infty)$.

The decreasing rate of $\mathcal{P}(\gamma, N)$ with respect to N can be formulated as

$$\zeta = \left| \frac{\partial \mathcal{P}(\gamma, N)}{\partial N} \right| = \frac{e^{-\frac{\gamma N}{\rho}}}{(\gamma+1)^{N-1}} \left(\frac{\gamma N}{\rho} + N \log(\gamma+1) - 1 \right), \ \gamma \geq 1.$$

In addition, the derivative of ζ with respect to N is expressed as

$$\frac{\partial\zeta}{\partial N} = -\frac{e^{-\frac{\gamma N}{\rho}}}{(\gamma+1)^{N-1}}\left(\frac{\gamma}{\rho} + \log(\gamma+1)\right)\left(\frac{\gamma N}{\rho} + N\log(\gamma+1) - 2\right), \tag{28}$$

which has a single zero at $N_0 = \frac{2}{\gamma/\rho+\log(\gamma+1)}$ and is negative on $[N_0;\infty)$. For $\gamma \geq 1$, we have $N_0 \leq \frac{2}{1/\rho+\log(2)} < \frac{2}{\log(2)} < 3$. Therefore, we can conclude that for the range $[3;\infty)$, ζ is a decreasing function of N.

We now prove that $\mathcal{P}(\gamma,N)$ decreases on $[2;3]$ faster than on $[3;4]$. The values of $\mathcal{P}(\gamma,N)$ at $N=2$, $N=3$, and $N=4$ are

$$\begin{aligned}
\mathcal{P}(\gamma,N)_2 &= \frac{2}{\gamma+1}e^{-\frac{\gamma}{\rho}}, \\
\mathcal{P}(\gamma,N)_3 &= \frac{3}{(\gamma+1)^2}e^{-\frac{2\gamma}{\rho}}, \\
\mathcal{P}(\gamma,N)_4 &= \frac{4}{(\gamma+1)^3}e^{-\frac{3\gamma}{\rho}},
\end{aligned}$$

respectively. From the decreasing property of $\mathcal{P}(\gamma,N)$, we have $\mathcal{P}(\gamma,N)_2 > \mathcal{P}(\gamma,N)_3 > \mathcal{P}(\gamma,N)_4$. Therefore, the decreasing rates of $\mathcal{P}(\gamma,N)$ on $[2;3]$ and $[3;4]$ are

$$\left|\frac{\Delta\mathcal{P}(\gamma,N)_{2,3}}{\Delta N}\right| = \mathcal{P}(\gamma,N)_2 - \mathcal{P}(\gamma,N)_3 = \underbrace{\frac{e^{-\frac{2\gamma}{\rho}}}{\gamma+1}}_{:=\alpha_1}\underbrace{\left(2 - \frac{3}{\gamma+1}e^{-\frac{\gamma}{\rho}}\right)}_{:=\beta_1}, \tag{29}$$

$$\left|\frac{\Delta\mathcal{P}(\gamma,N)_{3,4}}{\Delta N}\right| = \mathcal{P}(\gamma,N)_3 - \mathcal{P}(\gamma,N)_4 = \underbrace{\frac{e^{-\frac{3\gamma}{\rho}}}{(\gamma+1)^2}}_{:=\alpha_2}\underbrace{\left(3 - \frac{4}{\gamma+1}e^{-\frac{\gamma}{\rho}}\right)}_{:=\beta_2}, \tag{30}$$

respectively. We observe that

$$\frac{\alpha_1}{\alpha_2} = e^{\frac{\gamma}{\rho}}(\gamma+1) > 2,\ \gamma \geq 1, \tag{31}$$

$$\frac{\beta_2}{\beta_1} = 2 - \underbrace{\frac{1 - \frac{2}{\gamma+1}e^{-\frac{\gamma}{\rho}}}{2 - \frac{3}{\gamma+1}e^{-\frac{\gamma}{\rho}}}}_{:=\kappa},\ \gamma \geq 1.$$

Furthermore, we have $\frac{2}{\gamma+1}e^{-\frac{\gamma}{\rho}} < 1$, and $\frac{3}{\gamma+1}e^{-\frac{\gamma}{\rho}} < \frac{3}{2}$ as $\gamma \geq 1$, which lead to $\kappa > 0$, and hence

$$\frac{\beta_2}{\beta_1} < 2,\ \gamma \geq 1. \tag{32}$$

From (29) and (30), α_1, α_1, β_1, and β_2 are positive. Therefore, from (31) and (32), we have $\alpha_1\beta_1 > \alpha_2\beta_2$, which means that $\frac{\Delta\mathcal{P}(\gamma,N)_{2,3}}{\Delta N} > \frac{\Delta\mathcal{P}(\gamma,N)_{3,4}}{\Delta N}$. In other words, $\mathcal{P}(\gamma, N)$ decreases faster on $[2;3]$ than on $[3;4]$, which in conjunction with the decreasing property of $\zeta = \left|\frac{\partial\mathcal{P}(\gamma,N)}{\partial N}\right|$ on $[3;\infty)$ leads to the conclusion that $\mathcal{P}(\gamma, N)$ decreases more slowly with N on $[2,\infty)$. Thus, the proof of Remark 3.3 is complete.

Appendix B

.3 Proof of Theorem 4.1

Let us define $\check{\boldsymbol{h}}_n$ as the vector whose elements are the channel coefficients in (4.15), i.e., $\check{\boldsymbol{h}}_n = \left[\bar{h}_{1,n}, \ldots, \bar{h}_{N_r-\eta,n}\right]^T$ and $\check{\boldsymbol{R}}_r(\varepsilon_r)$ as the $(N_r - \eta) \times (N_r - \eta)$ covariance matrix of $\check{\boldsymbol{h}}_n$. Then, we have

$$\|\check{\boldsymbol{h}}_n\|^2 = \sum_{i=1}^{Nr-\eta} \left|\bar{h}_{i,n}\right|^2, \tag{33}$$

and $\check{\boldsymbol{h}}_n \sim \mathcal{CN}(0, \check{\boldsymbol{R}}_r(\varepsilon_r))$. With the Karhunen-Loeve representation, we can express $\check{\boldsymbol{h}}_n$ as

$$\check{\boldsymbol{h}}_n = \left[\check{\boldsymbol{R}}_r(\varepsilon_r)\right]^{\frac{1}{2}} \check{\boldsymbol{h}}_{w_n}, \tag{34}$$

where $\check{\boldsymbol{h}}_{w_n}$ has a distribution of $\mathcal{CN}(0, \boldsymbol{I})$ [36]. Now, by the eigenvalue decomposition, we have

$$\check{\boldsymbol{R}}_r(\varepsilon_r) = \boldsymbol{U}\boldsymbol{\Psi}\boldsymbol{U}^H, \tag{35}$$

where $\boldsymbol{U}$ is a unitary matrix and $\boldsymbol{\Psi} = \mathrm{diag}\{\xi_1, \ldots, \xi_{N_r-\eta}\}$ is a diagonal matrix whose diagonal elements are the distinct positive eigenvalues of $\check{\boldsymbol{R}}_r(\varepsilon_r)$.

From (34) and (35), $\|\check{\boldsymbol{h}}_n\|^2$ can be expressed as

$$\begin{aligned}\|\check{\boldsymbol{h}}_n\|^2 &= \check{\boldsymbol{h}}_n^H \check{\boldsymbol{h}}_n = \check{\boldsymbol{h}}_{w_n}^H \check{\boldsymbol{R}}_r(\varepsilon_r) \check{\boldsymbol{h}}_{w_n} \\ &= \check{\boldsymbol{h}}_{w_n}^H \boldsymbol{U} \boldsymbol{\Psi} \boldsymbol{U}^H \check{\boldsymbol{h}}_{w_n} = \left(\boldsymbol{U}^H \check{\boldsymbol{h}}_{w_n}\right)^H \boldsymbol{\Psi} \left(\boldsymbol{U}^H \check{\boldsymbol{h}}_{w_n}\right). \qquad (36)\end{aligned}$$

Let $\boldsymbol{v} = \boldsymbol{U}^H \check{\boldsymbol{h}}_{w_n}$. Then, since $\boldsymbol{U}$ is unitary, $\boldsymbol{v}$ has the same distribution as $\check{\boldsymbol{h}}_{w_n}$, i.e., $\boldsymbol{v} \sim \mathcal{CN}(0, \boldsymbol{I})$, and (36) can be rewritten as

$$\|\check{\boldsymbol{h}}_n\|^2 = \boldsymbol{v}^H \boldsymbol{\Psi} \boldsymbol{v} = \sum_{i=1}^{N_r-\eta} \xi_i |v_i|^2, \qquad (37)$$

where $|v_i|^2, i = 1, 2, \ldots, N_r - \eta$, are independent exponential random variables with unit means and variances. We define the random variable $\mathcal{Y}_n$ as $\mathcal{Y}_n = \|\check{\boldsymbol{h}}_n\|^2$. According to (37), $\mathcal{Y}_n$ has a generalized Chi-square distribution with a PDF and CDF of

$$f_{\mathcal{Y}}(y) = \sum_{k=1}^{N_r-\eta} \frac{e^{-\frac{y}{\xi_k}}}{\xi_k \prod_{i=1, i\neq k}^{N_r-\eta} \left(1 - \frac{\xi_i}{\xi_k}\right)}, \qquad (38)$$

$$F_{\mathcal{Y}}(y) = \int_0^y f_{\mathcal{Y}}(t) = \sum_{k=1}^{N_r-\eta} \frac{1 - e^{-\frac{y}{\xi_k}}}{\prod_{i=1, i\neq k}^{N_r-\eta} \left(1 - \frac{\xi_i}{\xi_k}\right)}, \qquad (39)$$

respectively [37]. From (4.15) and (33), we have

$$\mathcal{X}_{max,\mathrm{MMSE}} \approx \frac{\rho}{N} \max_{n=1,\ldots,N} \{\mathcal{Y}_n\}. \qquad (40)$$

Let $\mathcal{Y}_{max} = \max_{n=1,\ldots,N} \{\mathcal{Y}_n\}$. Then, (40) becomes

$$\mathcal{X}_{max,\mathrm{MMSE}} \approx \frac{\rho}{N} \mathcal{Y}_{max}. \qquad (41)$$

In the near semi-highly correlated channel, we have $\boldsymbol{R}_t(\varepsilon_t) \approx \boldsymbol{I}$. Therefore, $\check{\boldsymbol{h}}_n, n = 1, \ldots, N$, values are independent, and so are $\mathcal{Y}_n$ values. Thus, the CDF of $\mathcal{Y}_{max}$ can be given as

$$F_{\mathcal{Y}_{max}}(y) = [F_{\mathcal{Y}}(y)]^N = \left(\sum_{k=1}^{N_r-\eta} \frac{1 - e^{-\frac{y}{\xi_k}}}{\prod_{i=1, i\neq k}^{N_r-\eta} \left(1 - \frac{\xi_i}{\xi_k}\right)} \right)^N . \tag{42}$$

From (41) and (42), we obtain the CDF and PDF of $\mathcal{X}_{max,\text{MMSE}}$ as

$$\begin{aligned} F_{\mathcal{X}_{max,\text{MMSE}}}(x) &= F_{\mathcal{Y}_{max}}\left(\frac{N}{\rho}x\right) = \left(\sum_{k=1}^{N_r-\eta} \frac{1 - e^{-\frac{N}{\rho\xi_k}x}}{\prod_{i=1, i\neq k}^{N_r-\eta} \left(1 - \frac{\xi_i}{\xi_k}\right)} \right)^N , \qquad (43) \\ f_{\mathcal{X}_{max,\text{MMSE}}}(x) &= \frac{\partial}{\partial x} F_{\mathcal{X}_{max,\text{MMSE}}}(x) \\ &= \left(\sum_{k=1}^{N_r-\eta} \frac{1 - e^{-\frac{N}{\rho\xi_k}x}}{\prod_{i=1, i\neq k}^{N_r-\eta} \left(1 - \frac{\xi_i}{\xi_k}\right)} \right)^{N-1} \sum_{j=1}^{N_r-\eta} \frac{N^2 e^{-\frac{N}{\rho\xi_j}x}}{\prod_{i=1, i\neq j}^{N_r-\eta} \left(1 - \frac{\xi_i}{\xi_j}\right)}. \end{aligned}$$

This completes the proof.

.4 Proof of Theorem 4.5

For the sake of simplicity, we define the functions $\alpha(N)$ and $\beta(N)$ as

$$\alpha(N) = \frac{N^3}{\prod_{i=1, i\neq j}^{N_r-\eta} \left(1 - \frac{\xi_i}{\xi_j}\right)}, \quad \beta(N) = \sum_{k=1}^{N_r-\eta} \frac{1 - e^{-\frac{N}{\rho\xi_k}x}}{\prod_{i=1, i\neq k}^{N_r-\eta} \left(1 - \frac{\xi_i}{\xi_k}\right)}, \tag{44}$$

respectively. Then, the expression of $\mathcal{R}(N)$ in (4.25) can be rewritten as

$$\mathcal{R}(N) \approx \sum_{j=1}^{N_r-\eta} \alpha(N) \int_0^\infty \log\left(1 + x\right) e^{-\frac{N}{\rho\xi_j}x} \beta(N)^{N-1} dx. \tag{45}$$

From (4.20), we have $\mathcal{P}(x,N) = 1 - \left[F_{\mathcal{Y}}\left(\frac{Nx}{\rho}\right)\right]^N = 1 - \beta(N)^N$. Based on both the expression of the maximum SINR in (4.15) and Definition 2.1, we can conclude that $\mathcal{P}(x,N)$ increases with N_r. This is reasonable, because the use of more receive antennas results in a higher signal-combining gain as well as more efficient interference suppression at the MMSE receivers. Therefore, $\beta(N)$ decreases with N_r. For a fixed N with a large number of receive antennas, we have $\beta(N) \longrightarrow 0$. Hence, we can write

$$\mathcal{P}(x,N) = 1 - \beta(N)^N \approx 1 - \beta(N)^{N-1}, \tag{46}$$

For a small value of N_r, based on (44), we can write $\beta(N) \approx 1 - e^{-\frac{N}{\rho\xi_1}x}$. Since $\frac{N}{\rho} \longrightarrow \infty$, we get $\beta(N) \longrightarrow 1$. Hence, $\beta(N)^N \approx \beta(N)^{N-1}$, and (46) is also valid for this case. Therefore, we have $\beta(N)^{N-1} \approx 1 - \mathcal{P}(x,N)$. Now, we can rewrite (45) as

$$\begin{aligned}
\mathcal{R}(N) &\approx \sum_{j=1}^{N_r-\eta} \alpha(N) \int_0^\infty \log(1+x)\, e^{-\frac{N}{\rho\xi_j}x} \left[1 - \mathcal{P}(x,N)\right] dx \\
&= \sum_{j=1}^{N_r-\eta} \alpha(N) \left[\int_0^\infty \log(1+x)\, e^{-\frac{N}{\rho\xi_j}x} dx - \int_0^\infty \log(1+x)\, e^{-\frac{N}{\rho\xi_j}x} \mathcal{P}(x,N) dx\right]. \quad (47)
\end{aligned}$$

Let $\mathcal{I}_1$ and $\mathcal{I}_2$ be the first and second integrals in (47). It is clear that $\mathcal{I}_1$ and $\mathcal{I}_2$ both decrease with N; however, the latter decreases faster than the former due to the effect of $\mathcal{P}(x,N)$, which is also a decreasing function of N. This implies that $\mathcal{I}_1 - \mathcal{I}_2$ increases with N. In other words, $\mathcal{R}(N)$ is an increasing function of N, the optimal sum-rate is achieved at the maximum value of N, i.e., $N = N_t$, and the proof is complete.

요 약

본 논문에서는 대규모 다중입출력(MIMO) 시스템 하향링크을 위한 직교 랜덤 프리코딩 (Orthogonal Random Precoding) 기반의 커버리지 확장 기법을 연구하였다. 이 방식에서 사용자의 최대 신호대간섭잡음비를 향상시키기 위해 직교 벡터들로 구성된 프리코딩 행렬을 이용하여 신호를 송신한다. 직교 랜덤 프리코딩 방식의 성능을 분석하고 최적화하기 위해 다양한 수신기 구조에 대해 커버리지 확률 및 셀 경계 영역의 합계 전송 속도에 대한 분석식을 유도하였다. 이를 통해 적은 수의 프리코딩 벡터를 사용할 때 최적의 커버리지 성능을 달성함을 보였다. 또한 프리코딩 다이버시티(Diversity)를 이용하기 위해 서로 다른 랜덤 프리코더 그룹을 여러 시간에 걸쳐 이용하는 방식을 제안하였으며 해당 방식의 성능을 분석하였다. 유도한 분석식들이 직교 랜덤 프리코딩 시스템의 커버리지 성능을 정확하게 나타냄을 모의실험을 통해 보였다.

Acknowledgements

Firstly, I would like to express my sincere gratitude to my advisor, Prof. Kyungchun Lee, for the continuous support of my Master study and research. He inspires me to research and gives me the chance to pursue my passion. I could not have imagined having a better professor and mentor for my Master study.

Besides, I would like to thank Prof. Ji-Hoon Yun and Prof. Taehyun Jeon for kindly participating in my thesis defense and giving insightful comments on my thesis.

My sincere thanks also go to Dr. Do Trong Tuan for his kind recommendation for my Master course and always being a good example of a conscientious professor. I also would like to thank my teachers, Ms. Phuong, Luong, Giang, Trinh, Huong, who devotedly taught me from early stages of my academic career.

Last but not the least, I must express my very profound gratitude to my parents, brother, sister, and friends for providing me with unfailing support and spiritual encouragement throughout my years of study. This accomplishment would not have been possible without them.

Author

Nguyen Thanh Nhan